Sigma-coupled Charge-transfer Probes of the Fluoroprobe and Fluorotrope Type

CHAPTER · MAY 2007

DOI: 10.1007/0-387-23335-0_7

1 AUTHOR:

Jan W. Verhoeven
University of Amsterdam
268 PUBLICATIONS **8,752** CITATIONS

SIGMA-COUPLED CHARGE-TRANSFER PROBES OF THE FLUOROPROBE AND FLUOROTROPE TYPE

Jan W. Verhoeven*

7.1. INTRODUCTION

A plethora of optical probes based on charge-transfer (CT) is known. Evidently such probes must contain at least one moiety with electron donor properties (D) and at least one with electron acceptor properties (A). While in some cases intermolecular D/A complexes have been employed, in general D and A are either linked directly or via a conjugated pi-system (D–π–A). However, in this chapter the focus will be on some fluorescent probes in which D and A are linked by an extended sigma-system (D-σ-A) that prevents direct D/A contact but still allows electronic interaction via a through-bond mechanism.

In virtually all cases CT probes exploit the sensitivity of the spectral position or the intensity of a CT absorption band or a CT emission band for changes in the direct molecular environment of the D/A pair.

In the present chapter such changes will mainly be related to the solvating power and dynamics of that environment, but these are not the only properties which can be investigated with CT probes. Thus many CT probes have been reported which allow e.g. specific complexation of metal ions at the D site or protonation at that site. This typically reduces its electron donating properties thereby causing a significant blue-shift of the CT transition of the probe or even leads to a state inversion with the CT state no longer being the lowest excited state of the probe. The latter not only leads to dramatic changes in the absorption spectrum but especially also in the fluorescent behavior (e.g. switching from essentially non-fluorescent to strongly fluorescent). Examples of such probes are reviewed in other chapters of this series, but closer to the main stream of this chapter are the very well known polarity probes[1,2] based on the spectral shift ('solvatochromism') of a CT absorption or emission. Some examples of these have been compiled in Figure 7.1. The most prominent examples of solvatochromic CT absorption probes are the $E_T(30)$-probe and Kosower's Z-probe (see Figure 7.1).

* Jan W. Verhoeven, Laboratory of Organic Chemistry, University of Amsterdam, Nieuwe Achtergracht 129, 1018WS Amsterdam, The Netherlands.

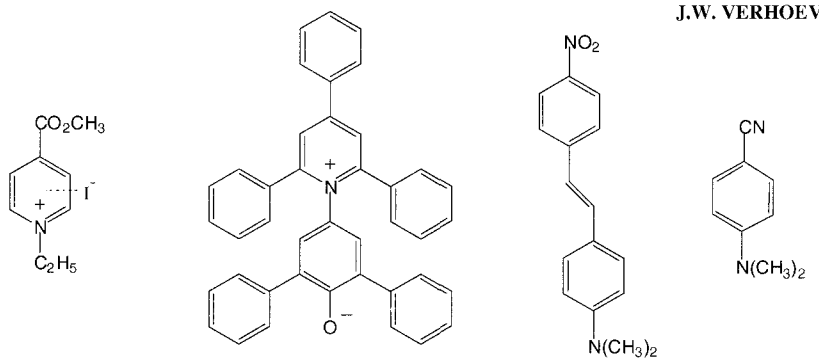

Z probe $E_T(30)$ probe DMANS DMABN

Figure 7.1. Typical charge-transfer probes with solvatochromic absorption and/or emission.

These probes have been used to define[1,2] the $E_T(30)$ and the Z-value solvent polarity scales, which simply reflect the position of the CT absorption maximum expressed in the somewhat odd units of kcal/mole. These CT absorption probes can be applied in virtually any solvent or solvent mixture (this is especially true for the closely related family of E_T probes) but of course suffer from the relatively low sensitivity of absorption measurements. This limits application in very small volumes and in highly scattering or absorbing media and makes remote monitoring quite difficult.

Evidently fluorescent CT probes could circumvent these limitations and in fact a plethora of such molecules has been reported, of which DMANS and DMABN are examples (see Figure 7.1). The transition responsible for their fluorescence has significant charge-transfer character and thereby makes the spectral position of that fluorescence sensitive to various changes in the molecular environment, which for the moment we will loosely indicate as polarity changes. Some of such molecules, such as DMABN, display dual fluorescence[3] from two states that differ in CT character and in conformation.

Before proceeding to the type of CT fluorescent molecules that are the subject of this chapter, a brief discussion will be given of the factors which govern the polarity dependence of CT probes in general. In doing so we will especially concentrate on the question how a maximum sensitivity (i.e. the largest spectral shift as a function of 'polarity') can be achieved.

7.1.1. Maximizing the Solvatochromism of CT Probes

The theory of solvatochromism has been treated extensively in many texts.[4] A crucial factor is always the difference in dipole moment between the ground and excited state of the probe molecule, which should be maximized. Furthermore strong solvatochromism in absorption requires that the ground state has a large dipole moment and the excited state a small dipole moment while strong solvatochromism in fluorescence requires the opposite. Thus the solvatochromic $E_T(30)$ and Z absorption probes shown in Figure 7.1 are essentially zwitterionic in the ground state and excitation in their CT absorption band leads to

(partial) cancellation of charges. Solvatochromic fluorescence probes contain D and A moieties which (ideally) are neutral in the ground state (D-A) and present a lowest CT excited state with zwitterionic character (D^+- A^-) from which the solvatochromic fluorescence stems.

Using a continuum dielectric model for the solvent and under the assumption that the dipole moment of the initial state (i.e. the ground state dipole moment μ_g for absorption probes and the excited state dipole moment μ_e for emission probes) is much larger than that of the final state the solvatochromism of absorption and emission probes can be expressed[4,5] via the relatively simple Eq. (1) resp. Eq. (2).

$$\nu_{abs} = \upsilon_0 + 10070\,(\mu_g^2/\rho^3)(f\text{-}f'/2) = \nu_0 + 10070\,(\mu_g^2/\rho^3)\Delta f = \nu_0 + S\Delta f \qquad (1)$$

$$\nu_{fl} = \upsilon_0 - 10070\,(\mu_e^2/\rho^3)(f\text{-}f'/2) = \nu_0 - 10070\,(\mu_e^2/\rho^3)\Delta f = \nu_0 - S\Delta f \qquad (2)$$

In these equations spectral positions are expressed in cm^{-1} and ν_0 stands for the (extrapolated) position of the absorption or emission maximum in the gas phase. The dipole moments (μ) are in Debye units and ρ (in Å) indicates the effective radius of the (spherical) solvent cavity surrounding the probe molecule. The solvent parameter Δf is defined on the basis of the bulk dielectric permittivity (ε) and the refractive index (n) as:

$$\Delta f = (\varepsilon\text{-}1)/(2\varepsilon\text{+}1) - (n^2\text{-}1)/(4n^2\text{+}2) \qquad (3)$$

Because of the definition of Δf it should of course be clear that the Eqs. (1) and (2) cannot be expected to describe correctly the influence of eventual specific solvation mechanisms such as hydrogen bonding. Nevertheless, and as we will see later on, the linear dependence predicted by Eq. (2) is often confirmed in the so called Lippert-Mataga plots of ν versus Δf over a wide range of solvent polarities where Δf varies between ca. 0.1 for saturated hydrocarbon solvents to ca. 0.4 for polar solvents like acetonitrile and the lower alcohols. The slope of such plots (S) is thus an objective measure for the polarity sensitivity of the probe employed at least as long as solvents giving specific interactions such as strongly hydrogen bonding solvents are excluded. Furthermore, for fluorescent probes S in principle carries quantitative information about the dipole moment of the excited state of the probe. Concerning the latter it should, however, be stressed that much uncertainty arises in determining an appropriate value for ρ, which is quite critical because S relates to the inverse cube of ρ. Probe molecules often have an elongated shape, which is thought to make the spherical cavity model underlying Eqs. (1) and (2) unsatisfactory. As an alternative Lippert proposed to set ρ at 40% of the long axis of an ellipsoidal cavity in which the probe fits. This may seem a small modification as compared to the spherical model where ρ is 50% of that axis, but for the same value of μ it predicts S to be almost twice as large and thus for the same value of S it leads to a calculated μ which is 1.4 times smaller than that derived via the spherical model! Nevertheless it is interesting to use the expressions given above for estimation of the maximum value that S might attain. In doing so we note that the length of a probe molecule (L) limits the dipole length it may contain to L-2d where d is the shortest distance between a center of charge in the dipole and the Van der Waals surface of the molecule as schematically indicated in Figure 7.2.

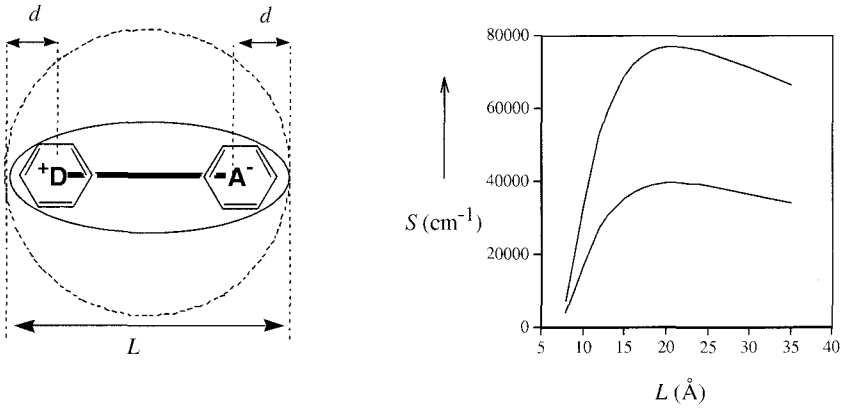

Figure 7.2. Spherical and ellipsoidal solvent cavity models for D-bridge-A molecules and the maximum solvent sensitivity (S) of their solvatochromic CT transition estimated therefrom as a function of the overall length (L) for d = 3.5 Å .

In most probes these charges are located in aromatic donor and acceptor moieties for which the Van der Waals radius $d \geq 3.5$ Å. In Figure 7.2 we now plot the slope S predicted by Eq. (2) as a function of the length of the probe assuming $d = 3.5$ Å and applying either the spherical cavity model where $\rho = 0.5L$ or the ellipsoidal cavity model with $\rho = 0.4L$.

While, as already noted above, the ellipsoidal model predicts S values that are twice those of the spherical model, both models indicate that S maximizes for probe molecules around 20Å in length. Although further elongation of course allows for larger μ values, its effect on the solvent sensitivity is offset and even overcompensated by the concomitant increase of ρ.

Quantitatively the graphs in Figure 7.2 should be taken with a 'grain of salt', but they demonstrate why extension of probe length may increase μ but not necessarily enhances the solvent sensitivity.

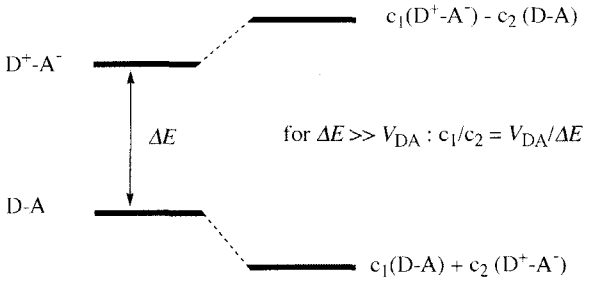

Figure 7.3. Mulliken two-state description of CT interaction.

$$V_{DA} = \frac{2.06x10^{-2}\sqrt{\varepsilon_{max}\upsilon_{max}\Delta\upsilon_{1/2}}}{R_c} \tag{4}$$

$$V_{DA} = \sqrt{\frac{1.4x10^{5}k_r}{n^3R_c^2\upsilon_{max}}} \tag{5}$$

In the discussion above it has tacitly been assumed that for a CT probe the CT transition switches the molecule between a state devoid of charge transfer (DA) and a state with full charge transfer character (D^+A^-). In most CT probes used (like the ones in Figure 7.1), however, these states mix to a certain degree and in fact the CT transition often derives a large part of its oscillator strength from such state mixing, which results from a non-zero electronic coupling (V_{DA}) between D and A. Thus the molar extinction coefficient (ε_{max} in $M^{-1}cm^{-1}$) of a CT absorption can be connected to V_{DA} via the well known Hush expression Eq. (4) and to the radiative rate constant (k_r) of CT fluorescence via the related Eq. (5).[6,7]

In these expressions V_{DA}, $\Delta\nu_{1/2}$ (the full bandwidth at half height), and ν_{max} are in cm^{-1}, k_r is in s^{-1}, while R_c represents the center-to-center distance of D and A in Å.
Both expressions are based on the Mulliken two-state model for CT interaction[8] in which the 'no-bond' DA configuration and the 'ionic' D^+A^- configuration mix to give the actual ground state and CT excited state as schematized in Figure 7.3.

This mixing reduces the difference in dipole moment between the two states and thereby the solvent sensitivity of CT probes. Especially for absorption probes this forms a problem because a strong CT absorption band is a desirable feature, but inevitably requires (see Eq. 4) a high value of V_{DA} and thus a relatively strong contribution (see Figure 7.3) of the CT configuration to the ground state wave function.

For fluorescent CT probes V_{DA} and thereby the degree of mixing can in principle be made much smaller. First of all because a high fluorescence quantum yield (Φ) may be achieved even when k_r is small if at the same time the radiationless decay rate (k_d) can be minimized because $\Phi = k_r/(k_r+k_d)$. And – as we shall see later – especially because the radiative rate can also be enhanced by mechanisms that do not require mixing of the DA configuration into the wavefunction of the CT radiative state.

7.2. SIGMA-COUPLED CHARGE TRANSFER PROBES; D-σ-A

7.2.1. Fluoroprobe (FP) an Extremely Solvatochromic Fluorescent D-σ-A Probe.

As we have seen above, the length of a CT probe and thus the distance between the D and A moieties should be limited for maximum sensitivity (see Figure 7.2) but at the same time also the electronic coupling V_{DA} between D and A should be limited.

For D-bridge-A probes in which the bridge is a conjugated pi-electron moiety (i.e. D–π–A) these two criteria are difficult to combine. A well studied example of a CT absorbing and fluorescent D-π-A probe is 4-dimethylamino-4'-nitrostilbene (DMANS, see Figure 7.1). The centers of the aniline donor moiety and the nitrobenzene acceptor moiety are about 6.7 Å apart, which suggests that in the CT excited state the dipole moment could increase by up to ≈ 32 D. However, D and A are strongly coupled via the ethylene pi–bridge and as a result the ground-state dipole moment of DMANS already has a high value (μ_g = 7.5 D) which increases with only ≈ 15.9 D in the excited state to μ_e = 23.4 D.[2] For longer pi–bridges the charges furthermore tend to become delocalised into the pi–bridge, which further offsets the change in dipole moment between ground and excited states.

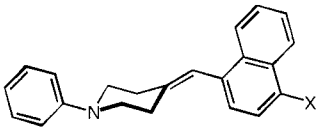

1 X= CN (Fluoroprobe, FP)
2 X = H

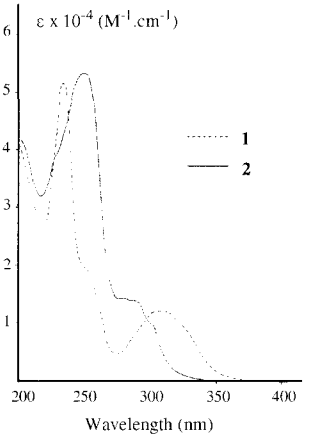

Figure 7.4. Structure of Fluoroprobe (**1**) and of its analogue **2** and their absorption spectra (in cyclohexane).

Early in our research on long-range electron transfer we found that saturated hydrocarbon bridges often allow remarkably fast photoinduced electron transfer to occur between D and A moieties connected by such bridges (i.e. D–σ–A) even if these bridges have a rigidly extended conformation which precludes direct D/A contact. Some of these systems even display discrete intramolecular CT absorption bands and some show CT fluorescence from the dipolar state thus populated upon excitation into that CT absorption or into local transitions of D or A.[9-11]

When D and A are neutral moieties - as in most systems we studied - their CT absorption shows very little solvatochromism but their CT fluorescence displays very pronounced solvatochromism, which is fully in line with the expected change from an essentially non-dipolar ground state (D–σ–A) to a dipolar CT excited state (D^+–σ–A^-). Regrettably the fluorescence quantum yield was in general quite low and often the CT fluorescence - if any - is only observable in a limited solvent polarity range. Evidently the through-sigma-bond interaction (TBI) responsible for the electronic coupling between D and A in extended D–σ–A systems is relatively weak thereby making the radiative rate (k_r) of the CT fluorescence in general too small to be of much practical importance for application of such systems as fluorescent probes.

This situation changed dramatically with the more or less serendipitous finding[12] of the molecule that was later dubbed 'Fluoroprobe' (FP) (**1**) followed by a series of analogues[13,14] such as **2** (see Figure 7.4).

Fluoroprobe contains an N,N-dialkylanilino electron donor moiety connected to a 1-vinyl-4-cyanonaphthalene electron acceptor moiety via a saturated piperidine bridge in an extended conformation. This structure implies that the D and A pi–systems are separated by at least three sigma-bonds and, as classically expected, the absorption spectrum of FP (see Figure 7.4) and its analogues thus provides little indication for any D/A interaction except perhaps for some broadening and tailing of the absorption spectrum towards the red, which might indicate the presence of a weak intramolecular CT absorption. In sharp contrast, however, the fluorescence spectrum of FP (as well as that of many of its analogues such as **2**) does neither display emission attributable to D nor to A but instead displays a strong structureless fluorescence with extreme solvatochromism attributed to intramolecular CT fluorescence.

Table 7.1. CT fluorescence maxima (ν_{ct} in cm^{-1}) of FP (**1**) and absorption maxima of the $E_T(30)$ probe in a series of 14 solvents. For comparison the $E_T(30)$ values given have been converted from kcal/mole to cm^{-1}.

Solvent	Δf	$E_T(30)$ (cm^{-1})	ν_{ct} (**1**) (cm^{-1})
1) n-hexane	0.092	10876	24600
2) cyclohexane	0.1	10841	24400
3) benzene	0.116	12035	20920
4) 1,4-dioxane	0.122	12631	19380
5) di-n-butylether	0.194	11578	21500
6) diisopropylether	0.237	11964	20400
7) diethylether	0.251	12105	19500
8) chloroform	0.251	13719	18830
9) ethylacetate	0.292	13368	17500
10) tetrahydrofuran	0.292	13122	17500
11) 1,2-dimethoxyethane	0.309	13403	16810
12) dichloromethane	0.319	14280	17300
13) pyridine	0.326	14210	15950
14) acetonitrile	0.393	15999	14400

Table 7.1 compiles data about the fluorescence maximum of FP in a series of 14 solvents and Figure 7.5 shows a Lippert-Mataga plot based on these data.

The most prominent feature is of course the extreme solvatochromism evidenced by a slope S = -35,000 cm^{-1} for FP, which brings it close to the theoretical maximum predicted via the spherical model although the ellipsoidal model suggests that there is still room for improvement (see Figure 7.2).

In Figure 7.5 we have also plotted as a function of Δf the $E_T(30)$ values of the solvents converted to a wavenumber scale. Evidently – at least in the nonhydroxylic solvents employed here – the sensitivity of the $E_T(30)$ probe is less than half that of FP. As predicted by Eqs. (1) and (2) the slope of the Lippert-Mataga plot is negative for FP and positive for $E_T(30)$. However, while for FP the correlation (with two exceptions, see Figure 7.5) is excellent, this is less so for $E_T(30)$. The smaller sensitivity of $E_T(30)$ and its weaker corre-

lation with Δf can probably both be related to the fact that in this probe strong mixing of the type indicated in Figure 7.3 occurs. Thus, while the ground-state dipole moment of the $E_T(30)$ probe is large (μ_g = 14.7 D), it remains rather large in the excited state (μ_e = 6 D)[2] and the assumption $\mu_g >> \mu_e$ underlying Eq. (1) therefore does not apply.

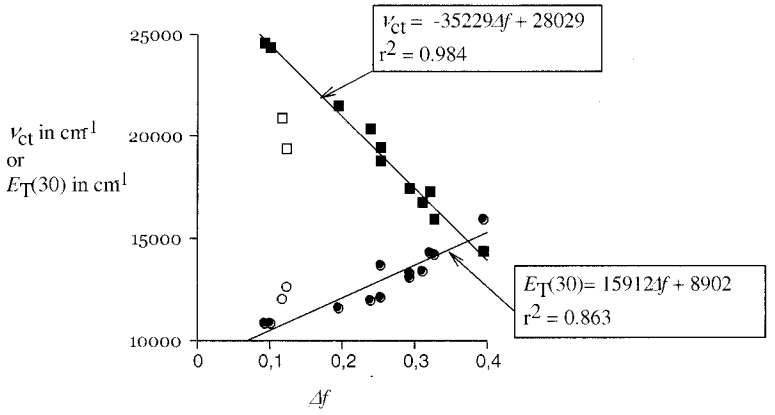

Figure 7.5. Lippert-Mataga plot (filled squares) for FP in a series of solvents. The correlation between Δf and the $E_T(30)$ values (filled circles) of the solvents is also shown. Benzene and 1,4-dioxane (open symbols) were omitted in the regressions.

By contrast the increase in dipole moment of FP in the excited state has been estimated from the Lippert-Mataga plot[12] as well as via other, independent techniques such as time resolved microwave conductivity (TRMC)[12] and electrochromism[15] to be as large as 27 ± 2 Debye. This huge increase in dipole moment corresponds to separation of two elementary charges at 5.6 ± 0.4 Å, which closely matches the distance between e.g. the C-1 atoms of the donor benzene and the acceptor naphthalene rings thereby substantiating the full CT character of the emitting state in FP.

As evident from Figure 7.5 the list of solvents (see Table 7.1) used contains two entries that do not fit the Lippert-Mataga plot. These are benzene and 1,4-dioxane, which both behave much more 'polar' than predicted by their Δf values. The anomaly of aromatic solvents and of 1,4-dioxane has been observed with many other polarity probes. It is generally agreed[4] that this anomaly is not related to specific solvent-solute interactions but stems from the fact that for close range interaction the nonspherical polarizability tensor of benzene and the quadrupolar nature of 1,4-dioxane become important to a degree not expressed in their bulk dielectric properties.

On the other hand specific interaction in the form of hydrogen bonding is probably involved in the strong quenching action of hydroxylic solvents on the fluorescence of FP. It is well known[4] that hydroxylic solvents also have a specific influence on other probes such as the $E_T(30)$ probe, which in alcohols shows a much stronger blue shift than would be predicted on the basis of bulk dielectric properties like Δf.

The extreme solvatochromism of FP implies a bathochromic shift of its fluorescence of $\Delta\upsilon$ > 10,000 wavenumbers upon transfer from cyclohexane to acetonitrile. Importantly

this shift occurs within the visible region (maxima ranging between 400 and 700 nm) which makes FP a very useful visible probe as may be clear from the photograph shown in Figure 7.6A, which displays the colors observed visually for various solutions of FP under UV illumination.

Figure 7.6A. (Please see Color Inserts Section) Fluorescence colors shown at room temperature by Fluoroprobe (FP) under UV illumination in a series of solvents with increasing polarity. From left to right : cyclohexane, benzene, toluene, 1,4-dioxane, chloroform, and pyridine.

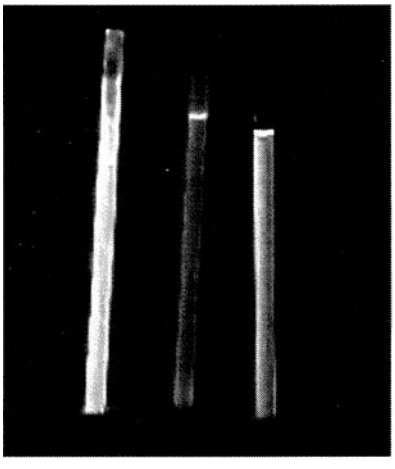

77 K 140 K 293 K

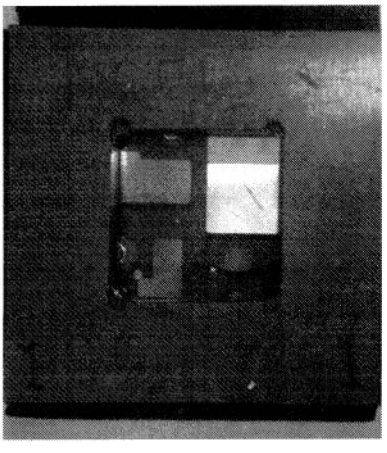

Figure 7.6B. Fluorescence of FP in MTHF at three temperatures. (Please see Color Inserts Section).

Figure 7.6C. Blue light emitted by a spin coated PLED based on **9** in PVK. (Please see Color Inserts Section).

Table 7.2. Fluorescence data of FP **1** and (in brackets) for **2** in various solvents at room temperature.

solvent	Δf	ν_{ct} (cm^{-1})	Φ	τ (ns)	k_r ($10^7\ s^{-1}$)	k_d ($10^7\ s^{-1}$)
n-hexane	0.092	24600	0.2	0.84	23.8	95.2
		(27300)	(0.06)	(0.17)	(35.3)	(553)
cyclohexane	0.1	24400	0.21	1.2	17.5	65.8
		(27300)	(0.06)	(0.2)	(30)	(470)
benzene	0.116	20920				
1,4-dioxane	0.122	19380				
di-n-butylether	0.194	21500	0.85	11.4	7.46	1.32
		(25800)	(0.19)	(1)	(19)	(81)
diisopropylether	0.237	20400	0.78	11.6	6.72	1.90
		(25100)	(0.28)	(2.1)	(13.3)	(34.3)
diethylether	0.251	19500	0.58	13,4	4.33	3.13
		(24300)	(0.46)	(4.5)	(10.2)	(12.0)
chloroform	0.251	18830				
ethylacetate	0.292	17500	0.19	7.3	2.60	11.1
		(22300)	(0.85)	(13.5)	(6.3)	(1.1)
tetrahydrofuran	0.292	17500	0.16	8.7	1.84	9.66
		(22400)	(0.74)	(13.9)	(5.32)	(1.87)
1,2-diMeO-ethane	0.309	16810				
dichloromethane	0.319	17300	0.21	8.3	2.53	9.52
		(21600)	(0.68)	(14)	(4.86)	(2.29)
pyridine	0.326	15950				
acetonitrile	0.393	14400	≈ 0.01			
		(19000)	(0.28)	(12.7)	(2.20)	(5.67)

7.2.2. Quantum Yields and Fluorescence Lifetimes of FP and Related Probes as a Function of Solvent

In Table 7.2 we have collected for FP and for the related probe **2**, which contains the weaker naphthalene instead of cyanonaphthalene acceptor (see Figure 7.4), some more fluorescence data.

These now include quantum yields (Φ), fluorescence lifetimes (τ) and the radiative (k_r) and dark (k_d) decay rates calculated from Φ and τ as: $k_r = \Phi/\tau$ and $k_d = (1/\tau)\text{-}k_r$. A collection of fluorescence spectra in various solvents is shown in Figure 7.7.

The absorption spectra of FP and **2** (see Figure 7.4) display only very minor solvent dependence but just like for FP also for **2** the fluorescence is CT in nature and displays extreme solvatochromism (S = - 27,400).

As might be expected, in each solvent the CT fluorescence of **2** occurs at significantly

higher energy than that of FP which simply relates to the higher energy of the CT excited state in the former. These observations have been made with many FP related probes[13,14] in which both the acceptor and the donor site were varied.

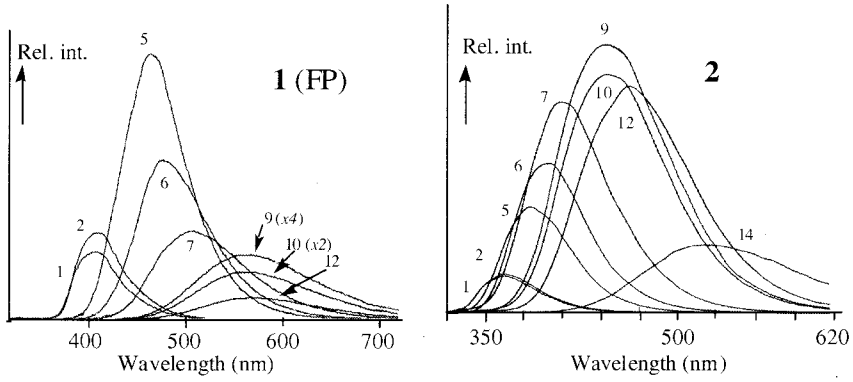

Figure 7.7. Fluorescence spectra of **1** (FP) and **2** in various solvents (see Table 7.1 for the numbering of solvents).

Another general observation, which deserves some more attention in the present context, is the solvent dependence of the quantum yield. This is plotted in Figure 7.8A as a function of Δf and in Figure 7.8B as a function of ν_{ct}. From Figure 7.8A it may be concluded that FP-like probes can be tuned to display their maximum fluorescence quantum yield in a certain polarity range, which has been substantiated by experiments with many such probes.

As already indicated by the data plotted in Figure 7.8B such maximum quantum yields always occur[13] in a polarity range where the combination of D and A incorporated in the probe leads to a fluorescence maximum around 22,000 cm^{-1} ($\approx$ 450 nm).

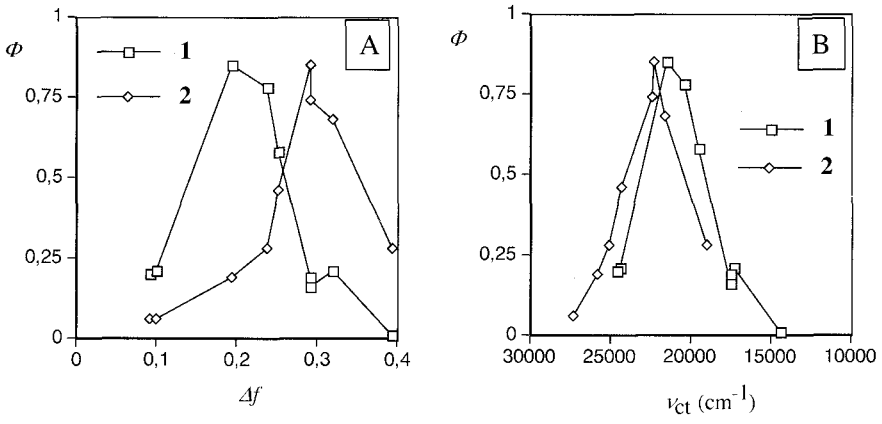

Figure 7.8. Fluorescence quantum yield as a function of solvent polarity Δf (A) and of the position of the fluorescence maximum ν_{ct} (B) for **1** (FP) and **2**. Lines are drawn between data points.

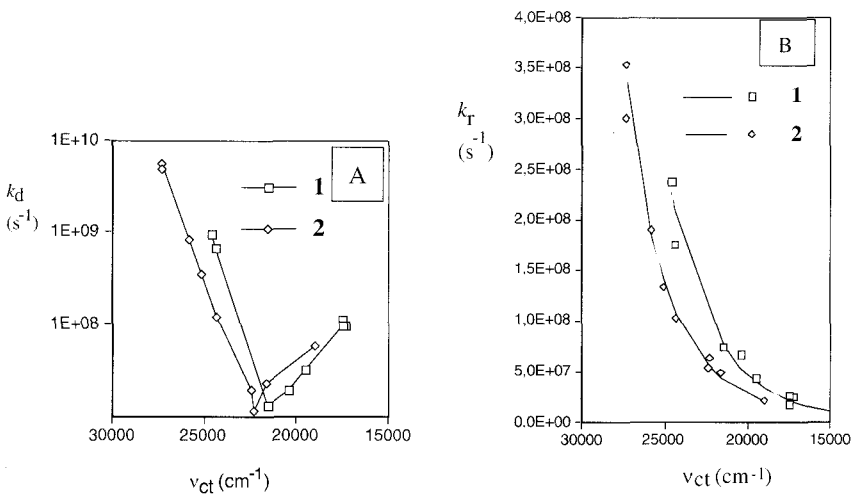

Figure 7.9. Dark decay (k_d) and radiative decay (k_r) rates for **1** (FP) and **2** as a function of the fluorescence maximum. Lines in Fig. 9A are drawn between data points, in Fig. 9B lines represent a best fit to Eq. (6), see text for details.

Closer inspection of the data in Table 7.2 reveals that this remarkable behavior is related to a strong dependence of both the radiative (k_r) and the dark (k_d) decay rates of the

CT excited state on the position of the CT fluorescence maximum. This is plotted for **1** and **2** (as representative examples of a large series of such systems investigated) in Figure 7.9A for k_d and in Figure 7.9B for k_r. As evident from Figure 7.9A k_d displays a minimum in the same range where the optimal quantum yield occurs and rises sharply (note the logarithmic scale) both in solvents where the fluorescence occurs at longer and at shorter wavelengths.

The increase of k_d in polar solvents, which induce a red shift, is not unexpected. This may simply be related to the energy-gap law, which implies that the vibrational coupling between an excited state and the ground state increases for smaller energy gaps thereby enhancing radiationless decay.

The sharp rise of k_d at higher energies, however, requires the contribution of an additional dark decay channel not directly leading to the ground-state. Originally we proposed[13] that this channel might be intersystem crossing from the CT singlet state to a local triplet state of the acceptor that is enhanced when the energy of the CT state rises to close the gap between these states. Later studies[16,17] have, however, made clear that instead a thermally activated[17] internal conversion to a local singlet state of the acceptor must be involved in which twisting of the exocyclic double bond of the acceptor occurs. This is a mechanism we suggested[11] earlier for other D–σ–A systems displaying a bell shaped dependence of the quantum yield of their (much weaker) CT fluorescence on solvent polarity. Interestingly, the nature of this mechanism implies that it can be suppressed by lowering the temperature as well as by increasing the viscosity of the medium, factors that thus increase the fluorescence quantum yield of FP-type probes especially under circumstances where it is blue shifted above 22,000 cm^{-1} (i.e. below $\approx$ 450 nm).

An equally remarkable solvent dependence is displayed by k_r (see Figure 7.9B), which increases strongly as the solvent is changed to induce a blue shift. It should be noted that this is the opposite of what is predicted by Eq. (5) based on the original Mulliken two-state model of D/A interaction (Figure 7.3), because upon increasing the energy gap between the ground and CT state their mixing should decrease leading to a concomitant decrease of k_r. Again, this non-Mulliken behavior of k_r has been observed by us for many D–σ–A systems. While a full discussion can be found in the literature[11,18,19] it suffices here to point out that instead of the simple two state model of Figure 7.3, a three (or more) state model adding one (or more) locally excited states of D or A seems required to describe the spectroscopic behavior of D–σ–A systems. In Figure 7.10 this is sketched for addition of a locally in A excited state (DA*).

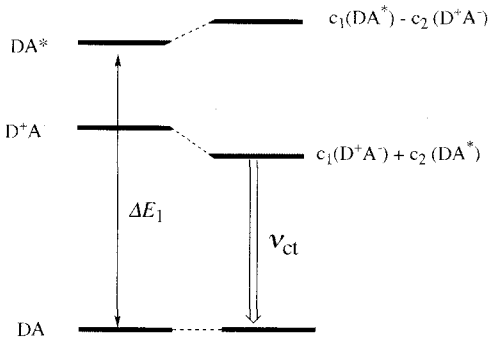

Figure 7.10. Three state model for D/A interaction leading to intensity borrowing by the CT transition from a local transition.

While we have analyzed this model allowing mixing between all three states[18,19] it has turned out that for D–σ–A systems the Mulliken-type mixing between DA and D^+A^- can often be neglected as compared to that between D^+A^- and DA*. This is not only due to the smaller energy gap between the two latter states, but probably also is related to the nature of the through-bond-interaction (TBI) in D–σ–A systems, which allows stronger interaction between higher energy states.

If – as assumed in Figure 7.10 – only mixing between excited configurations is taken into account the result is that the CT transition borrows most of its intensity from the local A→A* transition. If furthermore the mixing is relatively weak, the radiative rate of the CT fluorescence can be expressed by Eq. (6). Here ΔE_1 is the energy gap between the ground state and the locally excited state of A involved (see Figure 7.10), μ^* the transition dipole moment of the unperturbed A→A* transition and V_{DA^*} the electronic coupling matrix element between the D^+A^- and DA* configurations.

$$k_r = \frac{64\pi^4 n^3}{3h}(V_{DA^*}\mu^*)^2 \frac{\nu_{ct}^3}{(\Delta E_1 - \nu_{ct})^2} = Const.\frac{\nu_{ct}^3}{(\Delta E_1 - \nu_{ct})^2} \qquad (6)$$

In contrast to Eq. (5), Eq. (6) predicts that the radiative rate will rise sharply when the CT emission frequency shifts to the blue thereby reducing the energy gap between the CT state and the locally excited state. As can be seen in Figure 7.9B the radiative rates for FP and **2** as a function of the solvent induced shift can satisfactorily be fitted via Eq. (6) using ΔE_1 = 32,300 cm^{-1} for FP and ΔE_1 = 33,300 cm^{-1} for **2**. This corresponds to transitions at 310 nm and at 300 nm, which is close to the actual position of the first A→A* π–π* transition of the acceptor in FP and **2** (see Figure 7.4).

Further analysis[19] revealed that for FP the actual degree of mixing is small over the whole polarity range so that the emissive state retains its essentially complete CT character even in the most non-polar solvents where it was estimated that DA* contributes less than 10% to the emissive CT state, which nevertheless allows sufficient intensity borrowing from the strong A→A* transition to give the CT fluorescence a radiative rate $\geq 10^8$ s^-

[1] (see Table 7.2). Even in the gasphase[20] the fluorescence of FP is strongly CT in nature with ν_{ct} = 26,880 cm^{-1}, which is close to the position extrapolated from solution via the Lippert-Mataga plot shown in Figure 7.5. Interestingly studies under supersonic jet cooled conditions revealed[20,21] that under such conditions the lowest Frank-Condon excited state is local A* in nature and that a very small barrier ($\approx$ 100 cm^{-1}) separates it from the CT state, a barrier that disappears when the donor strength is enhanced by substitution with a *p*-methyl or *p*-methoxy substituent.[22]

The fact that little mixing between the ground-state and the CT state occurs is of course a very beneficial factor contributing to the extreme fluorescence solvatochromism of FP (and other D–σ–A probes) as compared to most D–π–A probes where the ground-state dipole moment is enhanced and the excited state dipole moment reduced by such mixing.

7.2.3. Improving the Absorption Characteristics of Fluoroprobe, from FP (1) to FT (3)

As evident from their absorption spectra (see Figure 7.4) efficient excitation of probes like FP and **2** requires light sources emitting rather deep in the UV. Although FP can still be excited in its absorption tail via the common 365 nm Hg line or with the frequency tripled output (355 nm) of a Nd-YAG laser, shorter excitation wavelengths such as produced by a nitrogen laser (337 nm) are more appropriate. This constitutes a drawback in some applications. Substitution of the naphthalene acceptor chromophore for larger aromatics such as anthracene and pyrene has been investigated[14, 21, 23] and has been found to lead to useful FP analogues absorbing at longer wavelength. However, the lowering of the DA* state resulting from such substitution also implies that it comes closer to the CT state and may even be lower in energy which implies that the CT fluorescence is substituted by a fluorescence with strong A*→A character. This was indeed observed[21,23] for such FP analogues in non-polar solvents and these analogues therefore display strongly solvatochromic CT fluorescence only in more polar media.

It should be borne in mind that when the CT state is the fluorescent state of a D/A system - like it is in FP - this also implies that excitation into the corresponding CT absorption should in principle constitute the longest wavelength excitation path of such a system unless extensive conformational reorganization occurs between the locally excited and CT state. Indeed the first absorption band of D–π–A systems, of directly coupled D–A systems, and of intermolecular D/A complexes (such as DMANS, E_T(30), and the *Z*-probe respectively, see Figure 7.1) is CT in nature. So why does FP not display a discrete intramolecular CT absorption band?

The expected position of the CT absorption maximum of FP can be estimated by assuming that the absorption band should show an approximate mirror relation with the fluorescence of FP in saturated alkane solvents (see Figure 7.7), which places it around 350 nm. Furthermore the oscillator strength of an absorption is in principle related to the radiative rate constant of the corresponding fluorescence, a relation which also connects Eqs. (4) and (5). In a simplified form this implies[24] that in the visible and near UV region the molar extinction of an absorption band and the radiative rate of the corresponding fluorescence are approximately related via Eq. (7):

$$k_r \approx 10^4 \, \varepsilon_{max} \tag{7}$$

Since (see Table 7.2) $k_r \geq 10^8$ s^{-1} for FP in non-polar solvents, this would imply that the CT absorption of FP should have $\varepsilon_{max} \approx 10^4$ ($M^{-1}cm^{-1}$). Although FP displays a distinct long wavelength absorption tail in the 350 nm region (see Figure 7.4) it is clear that this is much weaker than predicted.

The only way to explain this discrepancy is that the electronic coupling between D and A (i.e. V_{DA} in the two state model and V_{DA^*} in the three state model) is much weaker in the ground state than in the (relaxed) emissive state due to some conformational relaxation following or accompanying the intramolecular electron transfer.

In more flexibly linked systems this is often the result of conformational changes that reduce the D to A distance eventually driven by electrostatic attraction forces.[20,22,23,25-29] However, the very large and solvent independent dipole moment of the emissive state in FP makes it unlikely that this type of conformational processes occurs. Instead a more subtle conformational process seems to be involved, which selectively modulates the through-bond interaction between D and A. We assume that this occurs mainly via a change in the pyramidalization of the anilino nitrogen of the donor moiety. As substantiated by NMR and X-ray diffraction data[30] in the ground state of FP the central saturated piperidine ring adopts a chair conformation in which the donor nitrogen is pyramidalized with its phenyl ring in an equatorial orientation as expected from sterical considerations. This implies that the 'lone pair' orbital on that nitrogen occupies an axial position, which disfavors through-bond interaction with the acceptor pi-orbitals via the piperidine C-C sigma bonds. This is indicated in Figure 7.11 by the minor delocalization calculated for an axial lone pair in a model system (piperidone-4) where it can be seen that for an axial lone pair (hyperconjugative) delocalization of the lone pair occurs mainly into the properly aligned axial C-H bonds on the vicinal C2 and C6 atoms.

Enforcing an axial orientation of the N-substituent brings the lone pair in an equatorial position and thereby allows strong delocalization into the C2-C3 and C5-C6 bonds leading to significant TBI with the carbonyl group (which acts as the acceptor) via a path that closely fulfills the *all-trans* rule[31, 32] for optimal TBI. Also planarization of the nitrogen coordination (see central pictures in Figure 7.11) is predicted to lead to a strongly increased TBI.[32] Interestingly, such planarization is exactly what should occur in the CT excited state of FP because amine radical cations adopt a planar structure.[33-35]

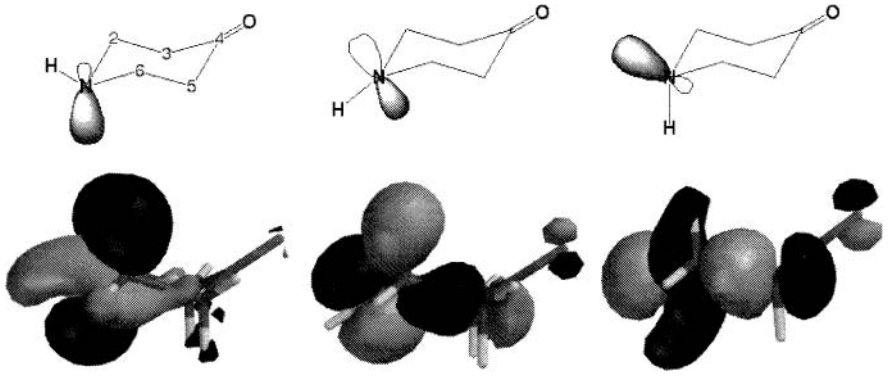

Figure 7.11. Three conformations of piperidone-4 and the calculated (AM1) effect on the delocalization of its (nitrogen 'lone pair') HOMO.

These qualitative considerations thus already provide a simple explanation for the apparent discrepancy between the high k_r of FP and its weak CT absorption. In the ground state the pyramidal structure around the anilino nitrogen and the equatorial orientation of the phenyl substituent allow only for weak TBI between D and A, but in the relaxed CT excited state planarization around the anilino nitrogen strongly enhances the TBI and thereby allows for a high k_r. Evidently this also implies that the CT absorption could be enhanced if the preferred ground state orientation of the phenyl substituent is changed from equatorial to axial. This has been achieved by expanding the Piperidine moiety to the bicyclic Tropane unit, leading to a system (see Figure 7.12) we named FluoroTrope (FT).[36] The additional ethylidene bridge in FT (**3**) sterically destabilizes the equatorial orientation of the phenyl ring and – as we have shown before[37-39] in systems containing stronger acceptor moieties – together with the additional stabilization of the axial orientation by TBI this suffices to make the axial orientation the preferred one in the ground state.

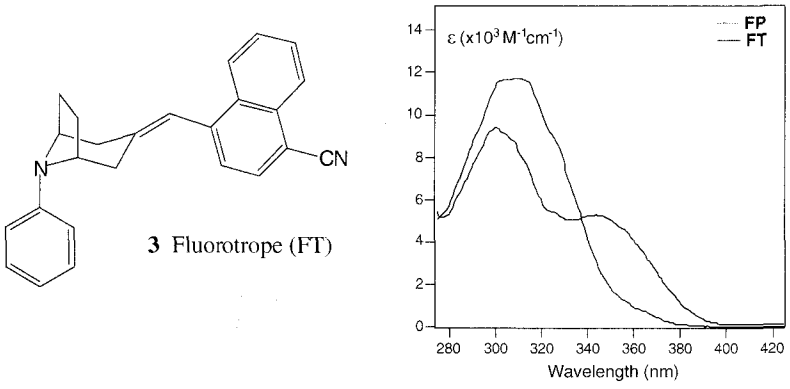

Figure 7.12. Structure of Fluorotrope (FT) and comparison of its absorption spectrum with that of FP (both in cyclohexane).

Comparison of the absorption spectra of FT and FP (Figure 7.12) confirms the dramatic increase of TBI in the former leading to the appearance of a discrete CT absorption band at the predicted position (350 nm) and with an intensity ($\varepsilon_{max} \approx 5000$ $M^{-1}cm^{-1}$) compatible with the k_r values found for FP. It is important to note that at the same time the first A→A* absorption of FT is weakened and blue shifted with respect to that in FP. This phenomenon has been observed[11] in many through-bond coupled D–σ–A systems and may be taken as strong evidence for dominant intensity borrowing of the CT transition from the local A→A* transition via the mechanism indicated in Figure 7.10. Again this implies that also in FT the degree of CT in the ground state can be very minor and that therefore its solvatochromism should be comparable to that of FP.

Table 7.3. Comparison of CT fluorescence maxima (ν_{ct} in 10^3 cm^{-1}), quantum yields (Φ), and fluorescence lifetimes (τ in ns) and radiative rates (k_r in 10^7 s^{-1}) for FT and FP.

	FT				FP			
Solvent	ν_{ct}	Φ	τ	k_r	ν_{ct}	Φ	τ	k_r
n-hexane	23.8	0.55	3.7	14.9	24.6	0.20	0.84	23.8
cyclohexane	23.7	0.61	3.9	15.6	24.4	0.21	1.2	17.5
di-n-pentylether	21.3	0.77	11.2	6.9				
di-n-butylether	21.0	0.74	11.5	6.4	21.5	0.81	11.4	7.1
di-n-propylether	20.7	0.72	12	6.0	20.4	0.78	11.6	6.7
diethylether	19.7	0.71	15.7	4.5	19.5	0.58	13.4	4.3
ethylacetate	17.6	0.25	6.7	3.7	17.5	0.19	7.3	2.6
tetrahydrofuran	17.5				17.5	0.16	8.7	1.8
dichloromethane	17.1				17.3	0.21	8.3	2.5

This is confirmed by the experimental results compiled in Table 7.3. These data demonstrate that FT and FP show a close similarity with respect to fluorescence position and quantum yield as a function of solvent. There are, however, a few differences that deserve comment. Both FP and FT display their strongest fluorescence (Φ around 80%!) in solvents of moderate polarity, but the decrease in quantum yield at lower polarity is less pronounced for FT than for FP. Thus FT retains $\Phi \geq$ 50% in saturated alkane solvents where for FP it drops to ca. 20%. As explained above the rather sharp drop of Φ in non-polar solvents must be attributed to the opening of a non-radiative path related to twisting of the exocyclic double bond of the acceptor when the CT state comes closer to the locally in A excited state. Fluorescence maxima of FT and FP in non-polar media indicate that in FT the CT state is at slightly lower energy and thus further removed from locally excited states than for FP in such non-polar environment. A very important conclusion to be drawn from the data in Table 7.3 is that – as visualized in Figure 7.13 – for any given position of the CT fluorescence maximum the radiative rate constants of FT and FP are virtually identical and both display the dependence on the energy of the emission maximum expected for a situation in which intensity borrowing from the local A→A* transition is dominant (see Eq. 6).

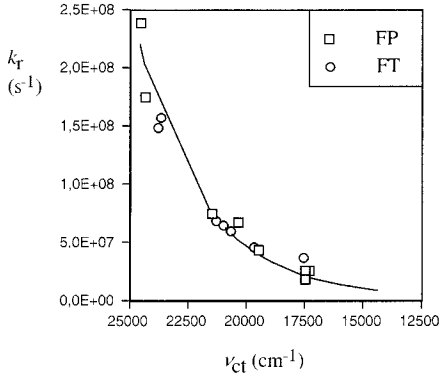

Figure 7.13. Comparison of the radiative rate constants of FP and FT as a function of their fluorescence maxima in a series of solvents (see Table 7.3 for data).

It may seem contradictory that FT and FP display similar radiative CT emission probabilities although the CT absorption is much stronger for FT than for FP. However, as already indicated above and as visualized in Figure 7.14, while the difference in CT absorption is caused by the difference in ground-state conformation, the conformation of the relaxed emissive CT state in FT and FP will be similar because the radical cation character of the donor in this state induces planarization of the anilino nitrogen.

In conclusion the results for FT show that it is possible to enhance significantly the long-wavelength absorption characteristics of FP without losing its uniquely strong solvatochromic properties.

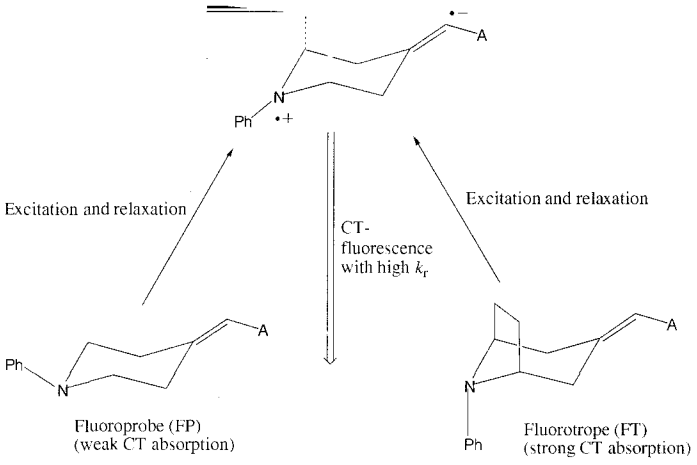

Figure 7.14. The conformation of FP and FT differs in the ground-state but is similar in the CT excited state resulting in very different CT absorption properties but nearly identical radiative CT fluorescence rates.

7.2.4. Fluorogenic Derivatives of FP and FT which Allow Covalent Attachment of the Probes; from FP and FT to MFP (4) and MFT (5)

In many applications it is desirable that optical probes can be attached covalently in a well defined location and especially for the investigation of biological systems many fluorescent probes have been extended with functional groups that allow them to form a covalent bond or eventually a very strong complex by reaction with specific functionalities in bio(macro)molecules.[40] Fluorogenic probes constitute a special class of such reactive probes. Fluorogenic probes are defined as being essentially non-fluorescent before reaction and showing strongly enhanced fluorescence after reaction. This property implies that the removal of unreacted probe molecules, which otherwise lead to nonspecific background fluorescence, can be omitted.

We decided to attach a maleimido group at the donor site of FP and FT because this group can be attached covalently to various nucleophilic centers and can also be copolymerized to become part of e.g. acrylic polymers as sketched in Figure 7.15.

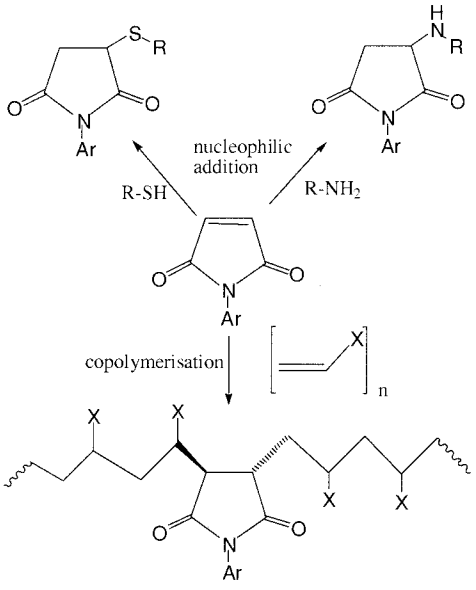

Figure 7.15. Reactivity of (N-aryl)maleimides converting the maleimide ring to a succinimide ring.

Furthermore it has been reported[40] that the maleimido group quenches the fluorescence of various fluorophores and that this fluorescence is restored upon reaction of the maleimido group.

This behaviour is dramatically demonstrated by the maleimido derivatives of FP and FT, named MFP[41] and MFT[36] depicted in Figure 7.16.

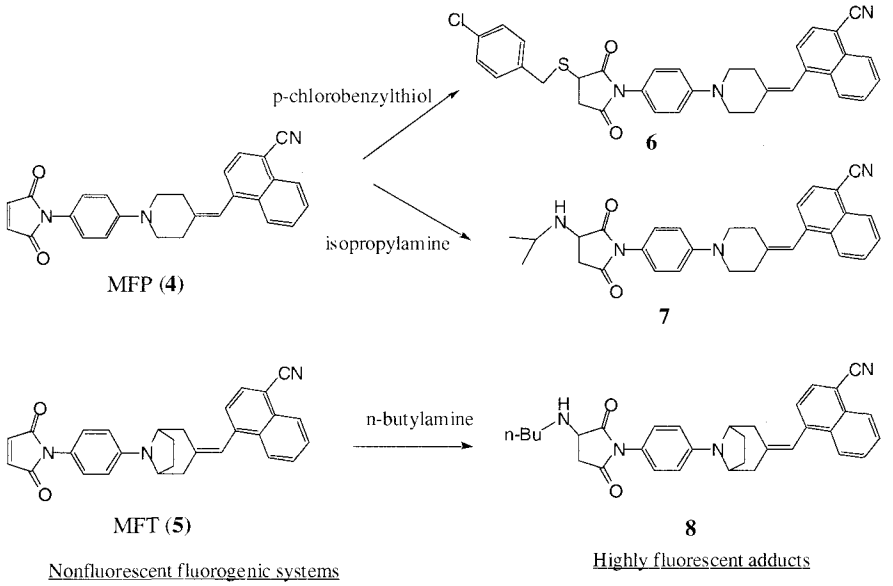

Figure 7.16. Structures of fluorogenic systems MFP and MFT and of their fluorescent adducts (**6**,**7** and **8**).

While as described above both FP and FT are highly fluorescent, MFP and MFT show no detectable fluorescence in any solvent. But after reactions of the type depicted in Figures 15 and 16 the strongly solvatochromic fluorescence of the FP or FT moiety is restored as shown by the data in Table 7.4, which compares fluorescence maxima of the adducts **6**, **7**, and **8** (see Figure 7.16 for structures) with those of FP and FT in a number of solvents.[36,41]

Table 7.4. CT fluorescence maxima (nm) of FP and FT compared to the adducts **6**, **7**, and **8** in various solvents.

	FP (**1**)	**6**	**7**	FT (**3**)	**8**
solvent			λ_{max}(nm)		
cyclohexane	410	411	411	420	420
di-n-butylether	465	466	461	476	a)
diethylether	513	518	516	508	503
ethylacetate	571	568	560	568	559
dichloromethane	578	564	559	585	575

a) Not determined

While the maleimido group thus exerts a strong quenching action, saturation of its double bond to yield a succinimide derivative removes this quenching and furthermore leads to a situation in which the donor capacities of the now para-substituted anilino moiety differ little from those in the parent FP and FT systems.

The latter finding is not unexpected because an N-succinimide substituent is estimated to exert little electronic influence since e.g. its Hammett sigma value (σ_p) is probably close to zero in analogy to other N-amido substituents.[42] The mechanism of the quenching action that the N-maleimide substituent exerts on FP and FT as well as on other fluorophores, such as pyrene[40] and electron rich stilbenes[40], seems to be not fully established yet. It has been noted[41] that N-phenylmaleimides show a very weak long wavelength absorption which shifts hypsochromically upon increasing solvent polarity and bathochromically upon introduction of electron releasing substituents on the phenyl ring. From the solvent effect this absorption was assigned to an n-π^* transition and the quenching effect was therefore tentatively attributed[41] to internal conversion populating such a low lying, non-emissive n-π^* state. On the other hand it has been noted[36,43] that maleimides have strong electron accepting properties. Semiempirical calculations[36,43] in fact suggested that in MFP and MFT the lowest unoccupied molecular orbital (LUMO) is not localized on the vinyl-cyanonaphthalene acceptor, as it is in FP and FT, but on the maleimido moiety. This implies that in MFT and MFP the lowest excited state is charge transfer in nature but with the maleimide acting as the acceptor. This is now further supported by the results of calculations on the model compound N-(4-dimethylamino phenyl)maleimide.

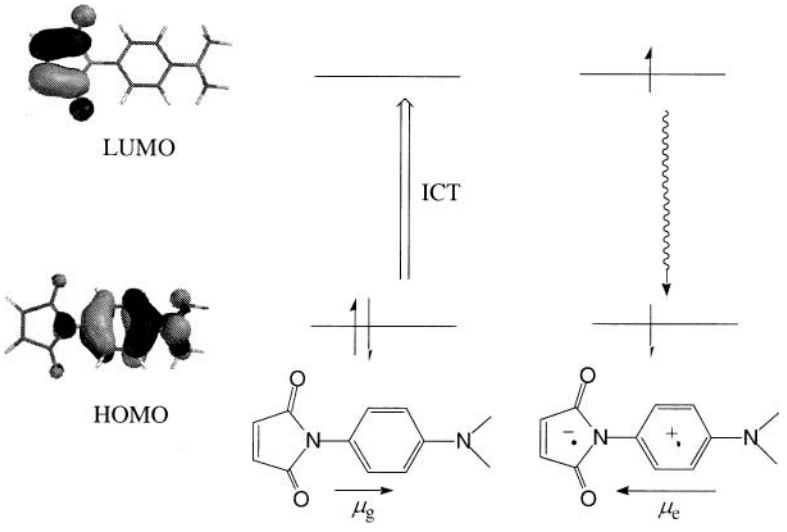

Figure 7.17. Frontier orbitals (AM1) of N-(4-dimethylaminophenyl)maleimide and the reversal of its dipole moment predicted to result from an ICT transition between these.

As shown in Figure 7.17 these calculations suggest that in this compound a weak internal charge transfer (ICT) transition should be available (weak because of the nodal properties of the HOMO and LUMO involved) leading to an apparently non-emissive CT state with a dipole moment oriented in a direction opposite to that of the (smaller) ground-state dipole moment. The inversion of the dipole moment is predicted to cause a

negative solvatochromism of the ICT absorption. This is because although more polar solvents stabilize the weakly dipolar ground state (μ_g calculated to be ca. 1.3 D) the orientation polarization of the solvent induced by the ground state dipole moment destabilizes to a larger extent the highly dipolar Franck Condon excited state. We therefore now propose that the weak long-wavelength absorption of some N-aryl maleimides, attributed earlier[41] to an n-π^* transition because of its negative solvatochromism, may in fact stem from such an ICT transition. For a model N-(4-dialkylaminophenyl)maleimide this absorption was found[41] at 380 nm (ε_{max} 300 $M^{-1}cm^{-1}$) in dichloromethane (390 nm in cyclohexane, 360 nm in methanol), which implies that the corresponding excited state is below the Franck-Condon CT state of FT (and FP) for which the CT absorption (which displays negligible solvatochromism) was found to occur around 350 nm (see e.g. Figure 7.12). Saturation of the double bond in the maleimide destroys its electron acceptor properties and thereby cancels the dark ICT state of the maleimide-donor moiety restoring the fluorescent CT state of the FT or FP probe as the lowest excited state.

7.3. APPLICATIONS OF D-σ-A PROBES

As already discussed above, FP, FT, derivatives of the fluorogenic MFP and MFT, as well as closely related systems in which the aromatic parts of D or A are modified or substituted can be employed as extremely sensitive polarity probes in a variety of liquid solvents. Also the behavior in solvent mixtures has been studied[21] revealing e.g. preferential solvation of the dipolar CT state by the most polar solvent component. The scope of application is, however, much wider than probing of micropolarity in liquid solution. Thus FP and some of its derivatives have been investigated isolated in a supersonically cooled molecular beam[20-22] and on the other hand have been attached covalently at a solid-liquid interface.[44] In this section, however, we will mainly concentrate on the behavior in complex media such molecular glasses, high molecular weight melts, (semi)crystalline solids, and polymers. We select here a number of examples of such studies to demonstrate the scope of FP and FT type fluorescent probes as well as their recently discovered electroluminescent properties.

7.3.1. Probing Solvation and its Dynamics as a Function of Temperature in Glass Forming Solvents

Until now we have tacitly assumed that the fluorescence observed from our probes stems from a relaxed CT state, which is at equilibrium with its surroundings. For (CT) absorption probes the assumption that their absorption occurs from a relaxed ground state is allowed, but with fluorescent probes after excitation unavoidably some emission already occurs before the nuclear reorganization of the surroundings as well as the internal reorganization of the probe itself have been completed. In low viscosity media at room temperature reorganization typically occurs on a (sub)picosecond time scale and thus for probes with nanosecond excited state lifetimes like FP and FT the contribution of fluorescence from non-relaxed states to the total emission is almost zero. Nevertheless, femtosecond time-resolved fluorescence studies of FP in liquid solvents have clearly shown the occurrence of a dynamic Stokes-shift over the first few picoseconds.[45,46]

At lower temperatures and especially when the solvent solidifies the reorganization is bound to slow down and thus fluorescence from non-relaxed states should become more important.

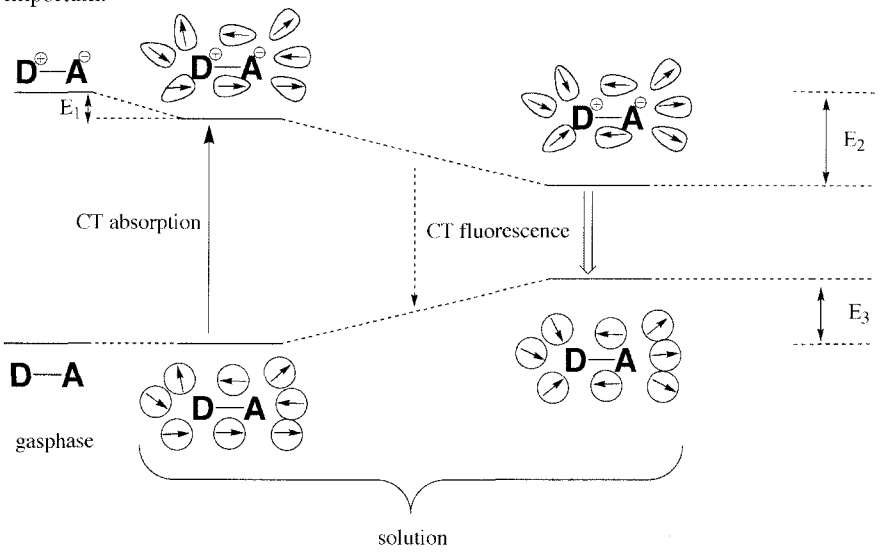

Figure 7.18. Solvation dynamics of a CT probe with zero ground-state dipole moment. Permanent solvent dipoles are indicated by small arrows, induced electronic polarization of solvent molecules is schematically indicated by a contour distortion.

Qualitatively this can easily be demonstrated by visual observation of solutions of FP or FT in dipolar solvents upon cooling down in e.g. liquid nitrogen. While under UV illumination at room temperature these solutions show a variety of colors depending on solvent polarity, as e.g. shown in Figure 7.6A, they all turn blue upon solidification as if solvent polarity is lost.

Figure 7.18 sketches the underlying dynamics of this process for a D-A system with zero ground state dipole moment and excited state dipole moment μ_e. In the ground state dipolar solvent molecules surround such a system randomly. Upon CT excitation in solution a Franck-Condon CT state is reached, which is (as compared to the situation for the isolated molecule) only stabilized by the rapid induced electronic polarization of the solvent molecules indicated in Figure 7.18 by a contour distortion. This stabilization amounts to:

$$E_1 = -(\mu_e^2/\rho^3)\{(n^2-1)/(2n^2+1)\} = -(\mu_e^2/\rho^3)f' \qquad (8)$$

It is interesting to note that according to Eq. (8) D-A systems with zero ground state dipole moment should show a significant red shift of their CT absorption upon transfer from the gasphase ($n^2 = 1$) to solution but that variation of the solvent should lead to minor further solvatochromism because the refractive index of common solvents varies little from $n^2 \approx 2$.

As sketched in Figure 7.18, orientation polarization of the solvent dipoles leads to further stabilization of the dipolar CT state, which after full relaxation increases to:

$$E_2 = -(\mu_e^2/\rho^3)\{(\varepsilon\text{-}1)/(2\varepsilon\text{+}1)\} = -(\mu_e^2/\rho^3)f \tag{9}$$

Fluorescence from a fully relaxed situation then leads to a Franck-Condon ground state in which the electronic polarization of the solvent is lost but its orientation polarization is still retained. This causes it to be destabilized by:

$$E_3 = +(\mu_e^2/\rho^3)\{(\varepsilon\text{-}1)/(2\varepsilon\text{+}1) - (n^2\text{-}1)/(2n^2\text{+}1)\} = +(\mu_e^2/\rho^3)(f - f') \tag{10}$$

Combination of Eqs. (9) and (10) directly leads to the Lippert-Mataga equation (Eq. 2) mentioned earlier, in which it is thus assumed that the fluorescence observed stems from a fully relaxed CT state, which is a valid assumption for low viscosity media at ambient temperature. As indicated by a dashed arrow in Figure 7.18, fluorescence from an incompletely relaxed situation should be blue shifted to a degree depending on the degree of relaxation and thus its time dependence (i.e. a dynamic Stokes shift) provides direct information about the solvation dynamics.

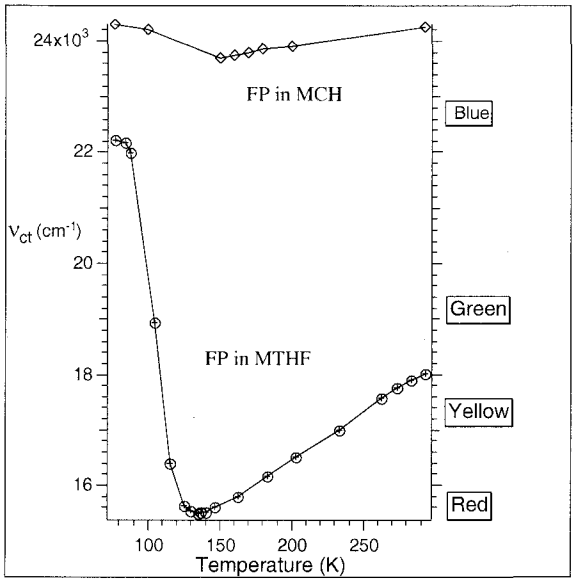

Figure 7.19. Continuous fluorescence maximum as a function of temperature for FP in 2-methyltetrahydrofuran (MTHF) and in methylcyclohexane (MCH).

The temperature dependence (see Figure 7.19) of the fluorescence of FP in the glass forming polar solvent 2-methyltetrahydrofuran (MTHF) and in the non-polar solvent methylcyclohexane (MCH) provides a striking demonstration of the solvation dynamics sketched in Figure 7.18.[47] While in MCH the fluorescence maximum of FP was found to stay within the narrow range of 24,000 ± 200 cm^{-1} over the temperature range 77-300K, in MTHF (see Figure 7.19) the FP fluorescence traverses a range of about 7000 cm^{-1} spanning the visible spectrum as also demonstrated by the color photographs shown in Figure 7.6B.

At 293 K an MTHF solution of FP shows strong green-yellow fluorescence with a maximum located at 562 nm (17,800 cm^{-1}) and a fluorescence lifetime of τ = 12.6 ns. Upon cooling the fluorescence gradually shifts to the red (over more than 100 nm!) with an average of 15 cm^{-1}/K until a bright red color is attained around 140 K. It turns out that this red-shift can be reproduced quite well by the Lippert-Mataga equation (Eq. 2) taking into account the increase of the dielectric constant (ε) and the refractive index (n) at lower temperatures. Microscopically this can be understood from the increased density of the solvent and from the increased dipolar orientation of the solvent molecules with respect to the solute dipole as the counteracting thermal motions diminish upon cooling.[4]

The fact that the Lippert-Mataga equation applies down to ca. 140 K implies that over this temperature range the solvent reorganization remains fast as compared to the fluorescence lifetime of FP.

Below 140 K the red-shift first levels off and below 130 K changes to a very dramatic blue-shift that in the region 120-90 K amounts to -153 cm^{-1}/K and levels off again at lower temperatures. It is known[48] that the solvent relaxation time of MTHF increases to nanoseconds upon cooling into the supercooled liquid region (i.e., below the melting point of T_M = 135 K) and rapidly increases further to seconds upon cooling to the glass transition point $T_G \approx 91$ K. That as a result below 140 K a sizable fraction of the overall fluorescence occurs from not fully relaxed states can easily be shown from the fact that in this region the fluorescence displays a time dependent Stokes shift (see Figure 7.20), which extends over periods ranging from a few nanoseconds at 130 K to way over 40 ns (the maximum time window in which fluorescence can be detected) below 110 K.[47]

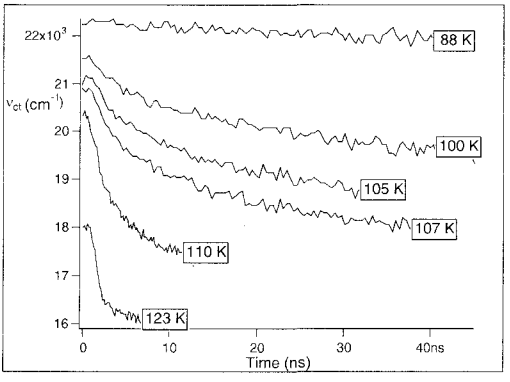

Figure 7.20. Dynamic Stokes shift of the CT fluorescence of FP in MTHF at various temperatures (excitation at 337 nm with 600 ps (fwhm) nitrogen laser pulses).

The measurements described above for FP in MTHF and MCH were also performed[49] for a solution of FP in sucrose octaacetate (SOA). When molten (melting point ca. 360 K) SOA behaves as a viscous liquid which solidifies to a clear glass upon cooling. In fact (see Figure 7.21) the thermochromic shift of FP in SOA is qualitatively similar to that in MTHF, but occurs at much higher temperatures. A noticable difference between the situation in SOA and in MTHF is that in SOA in the 300-400 K region the shift of the maximum only amounts to ca. -25 cm^{-1}/K whereas in the 'undercooled liquid' region in MTHF this shift was over -150 cm^{-1}/K. This difference is probably brought about by the higher thermal energy in the SOA matrix as compared to the undercooled MTHF, making it harder to freeze nuclear relaxation processes in SOA. This is also indicated by the results of time resolved measurements (see Figure 7.21) on the shift of the FP emission maximum after pulsed laser excitation. It turns out that over most of the temperature region investigated including the viscous liquid region above the melting point and even down to 300 K, where SOA forms a mechanically very hard glass, a significant dynamic Stokes shift occurs over a time window spanning more than the fluorescence lifetime. This implies that the continuous fluorescence spectra, of which the maxima are plotted in Figure 7.21, are always a weighed average over the time domain in which emission occurs. Furthermore these results show that at room temperature significant nuclear reorganization processes can still take place in a very hard matrix on a nanosecond time scale. We will come back to this phenomenon later in this chapter.

The observations described in this section demonstrate that, in contrast to CT absorption probes, fluorescent CT probes cannot only detect changes in the solvating power of the medium but are also able to provide direct information about the local mobility of the medium. For FP like probes the resulting thermochromism in a suitably chosen medium easily spans the whole visible range of the spectrum and can act as a 'molecular-scale thermometer' of which the temperature range and sensitivity can be tuned by changing the medium directly surrounding the probe.

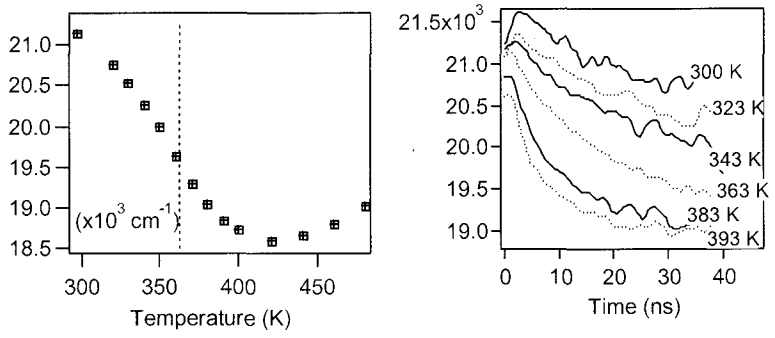

Figure 7.21. Continuous fluorescence maximum of FP in sucrose octaacetate (SOA, melting point indicated by vertical dashed line) as a function of temperature (left) and the dynamic Stokes shift observed after laser excitation (337 nm, fwhm 600 ps) at various temperatures.

7.3.2. Probing of Mobility Changes and Phase Transitions in (Semi)Crystalline Materials

The experiments in the previous section related to the transition between liquid solutions and an amorphous, glassy matrix. As expected from the decreased molecular mobility such a transition is always reflected by a blue shift of the fluorescence of our CT probes. Furthermore, in the solid glassy matrix cooling always leads to a further blue shift, the extent and steepness of which depends on the type of medium involved and the temperature domain over which the glassy state exists.

Striking deviations from this behavior have been observed for a number of transitions between the liquid and (semi) crystalline state as well as for the temperature dependence in that crystalline state. A few examples of such observations will now be described.

7.3.2.1. Octadecyl octadecanoate (Stearylstearate), CH_3-$(CH_2)_{17}$-O-(CO)-$(CH_2)_{16}$-CH_3

This is a crystalline solid at room temperature and in its melt (mp 334 K) FP can readily be dissolved to give a strongly fluorescent solution.[50] Further heating of this solution leads to a gradual blue shift in analogy with the thermochromism in other solvents (see above). However, upon crystallization instead of the expected blue shift a significant red shift occurs from ≈ 460 nm at 334 K to ≈ 495 nm at 310 K. Further cooling then induces a gradual blue shift (to e.g. 440 nm at 220 K). We suspected that this behavior is related to a solid state phase transition, but DSC (differential scanning calorimetry) did not reveal the existence of such a transition and only showed a sharp melting at 334 K. However, temperature dependent wide angle X-ray scattering (WAXD) revealed that a phase transition indeed takes place and occurs about 20 K below the melting point. While this explains why below this point FP shows the expected blue shift upon decreasing temperature it remains to be explained why the transition from the liquid to the solid state is accompanied by a red shift. Clearly the crystalline state initially formed is metastable and only exists over a small temperature domain of ca. 20 K. It must be concluded that during its formation from the melt the FP molecules are incorporated in such way that the medium dipoles are fortuitously already pre-oriented so as to stabilize the CT excited state better than can be achieved via the dipolar field induced orientation in the liquid state. That this pre-orientation is far from optimal can be concluded from the very significant dynamic Stokes shift that FP undergoes in solidified octadecyloctadecanoate.[50,51]
Similar observations were made[51] with ethylstearate (C_2H_5-O-(CO)-$(CH_2)_{16}$-CH_3).

7.3.2.2. α,ω-Diacetyl polyethyleneglycols, CH_3CO-$(OCH_2CH_2)_m$-$OCOCH_3$

The occurrence of a dynamic Stokes shift in solid matrices is a recurring theme and while a discussion of the underlying mechanism will be postponed to a later point it is clear that this must be related to a certain mobility of the matrix and/or the probe. This mobility cannot only be varied by temperature - as shown above - but also by e.g. varying the molecular weight of the matrix molecules such as was done in a series of homologous α,ω-diacetyl polyethylene glycols CH_3CO-$(OCH_2CH_2)_m$-$OCOCH_3$ with m = 2-225.[51-55] At room temperature the lower members in this series are viscous liquids, the higher members are waxy to crystalline solids. Over the whole range of m values investigated, including the solid regime, a distinct blue shift of the fluorescence maximum of FP was

observed with increasing molecular weight. Comparison with the behavior of FP in low viscosity binary mixtures of ethylacetate and diglyme containing increasing mole fractions of the latter suggests that in the absence of mobility restrictions the fluorescence in fact should shift to the red for higher *m*. Coupled with the observation[51,53,54] of significant dynamic Stokes shifts in a time window up to 60 ns, this implies that the blue shift is governed by a decreasing mobility over the whole molecular weight range investigated including that of the solid members.

7.3.2.3. Thermal and Mechanical Effects in Copolymers and Block-copolymers

Copolymers and especially block-copolymers have a complex morphology related to the presence of microdomains that vary from completely amorphous to highly crystalline. The behavior was investigated[51,56] in some depth of FP as a function of temperature and of mechanical stress in a number of such block-copolymers having molecular weights in the range 30,000 – 60,000 composed of alternating blocks of polybutylene terephthalate (PBT) and polyethylene glycol (PEG). In mechanical stretching experiments it was found that the FP fluorescence maximum undergoes significant and partly reversible spectral shifts and that the magnitude as well as the sign of these shifts depends strongly on the mechanical and thermal pretreatment of the samples. In thermographic (DSC) measurements the PBT/PEG copolymers display various phase transitions which can e.g. be related to melting of the PEG resp. PBT regions. Interestingly, all of these phase transitions are reflected by significant changes in the continuous fluorescence maximum of FP incorporated in these copolymers.

7.3.3. Probing of Polymerization Processes

As shown above, the fluorescence of CT probes is not only sensitive to the polarity but also to the mobility of the medium. It was realized that this should enable us to detect the progress of a polymerization process and as early as 1987 this was indeed demonstrated[57] by monitoring the fluorescence of FP dissolved in the monomer methylmethacrylate (MMA) during thermal polymerization to give PMMA. In MMA at room temperature the fluorescence of FP occurs at 565 nm (17,700 cm^{-1}), which compares well with that observed (see Table 7.1) in e.g ethylacetate. After polymerization to PMMA the fluorescence maximum has shifted dramatically to the blue (ca. 450 nm at 293 K) which can mainly be attributed to the reduced mobility.

Similar observations were made during polymerization of several other monomers.[51] In all cases, however, the majority of the shift occurs over a small part of the overall polymerization process since it sets in only when the polymerization has progressed sufficiently to increase significantly the viscosity (i.e. during the gelation and vitrification stages). This limitation has more recently been removed by the use of the fluorogenic derivatives MFT and MFP. As sketched in Figure 7.15 the maleimide group of MFT and MFP can enter into copolymerization with acrylic monomers. This reaction both triggers the fluorescence and makes the fluorescent probes a part of the growing polymer chain. Recent studies by us[58,59] and by others[60] of radiation induced polymerization of MMA have demonstrated that this allows monitoring of the full polymerization process. In the early stages only the fluorescence intensity rises from zero while the position remains constant as the probe is incorporated in the growing chain without significant viscosity

increase. In later stages (just like with FP) also a sharp blue shift upon gelation and vitrification occurs.

Already during the earliest polymerization experiments[57] with FP in (P)MMA it was noted that in PMMA the FP fluorescence undergoes a dynamic Stokes shift extending over a time domain up to 50 ns. This implies that most of the fluorescence stems from non-relaxed states and that the spectrum observed by continuous spectroscopy is a weighed average of those emitted during relaxation. As a result the continuous fluorescence maximum of FP in PMMA was found to be rather temperature dependent shifting to the red at higher temperatures where relaxation is faster (ca. 430 nm at 110 K, 450 nm at 293 K, 490 nm at 433 K, the latter being well above the glass transition point $T_g \approx 393$ K). This latter finding already makes it unlikely that the dynamic Stokes shift observed stems from an inhomogenenous distribution of sites in the PMMA homopolymer occupied by FP molecules in such a way that those emitting more to the red have a longer fluorescence lifetime. Recent studies by Frahn et al.[60] further support that the dynamic Stokes shift in PMMA stems from relaxation processes and not from inhomogeneity. Both for FP in PMMA and for MFP incorporated covalently in PMMA very similar dynamic Stokes shifts and shift kinetics were found. Furthermore it was observed that at the red side of the spectrum the emission shows a distinct growth during the first nanoseconds after excitation, which occurs over the same time domain as a fast component of the decay at the blue side (see Figure 7.22).

This is fully in line with a real dynamic Stokes shift from a homogeneous collection of sites just like in the amorphous glassy matrices like MTHF, MCH and SOA discussed earlier. An interpretation problem still arises from the fact that the time scale of the relaxations indicated by these Stokes shifts is much shorter than that of the fastest relaxation processes detected by e.g. dielectric relaxation measurements[61] on polymers like PMMA. Initially it was suggested[57] that internal relaxation processes of the probe might be involved rather than reorganization processes in the matrix. However, the lack of a significant shift upon cooling a non-polar matrix like MCH from the liquid to the solid state (see Figure 7.19) makes it unlikely that this plays an important role and/or implies that internal reorganizations such as the planarization of the donor nitrogen (see Figure 7.14) remain very fast even in solid matrices.

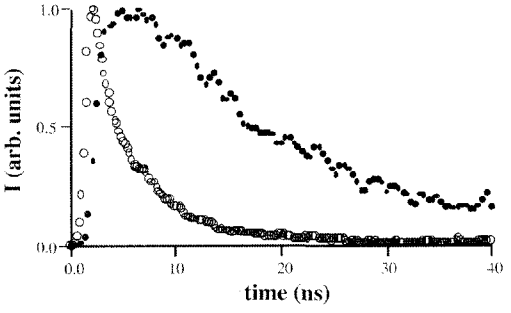

Figure 7.22. Fluorescence decay curves monitored[60] at 380 nm (circles) and at 580 nm (dots) after pulsed laser excitation (337 nm, fwhm 500 ps) of FP in PMMA at room temperature. Note the fast decay at the short wavelength extreme of the emission and the growth followed by a much slower decay at the long wavelength extreme.

Alternatively it was suggested[55] that the dynamic Stokes shift of FP like probes in polymers might be related to reorientation of the probe with respect to the surrounding polymer in the free volume occupied by the probe. While fluorescence depolarization measurements[57] show that such reorientation cannot be excluded, the recent observation by Frahn[60] that for FP in PMMA and for covalently attached MFP in PMMA the magnitude and kinetics of the dynamic Stokes shift are virtually identical also seems to exclude such reorientation as a major source of the dynamic Stokes shift observed. As a way-out it has been proposed by Frahn et al.[60] that the strong dipolar field created by the CT excited state of the probe could accelerate reorientation of polar side groups of the surrounding polymer to occur on a nanosecond time scale rather than on the much longer time scales concluded from e.g. dielectric relaxation measurements. It remains to be seen whether this probe-effect is operative or whether certain rapid microscopic motions in polymers detectable with CT fluorescent probes have until now just escaped observation by other techniques.

7.3.4. Penetration of Solvents and Vapors in Polymers

Small molecules can penetrate many polymers from the liquid or gaseous phase. An example of this is the swelling of polymer particles dispersed in an aqueous solution ('latices') upon addition of certain organic solvents, which can be followed by monitoring the particle size via quasi-elastic light scattering (QELS) or scanning electron microscopy (SEM). For a monodisperse ($\varnothing \approx 400$ nm) polystyrene latex such QELS data are shown in Figure 7.23 with dichloromethane (DCM) as the swelling agent.[51,62]

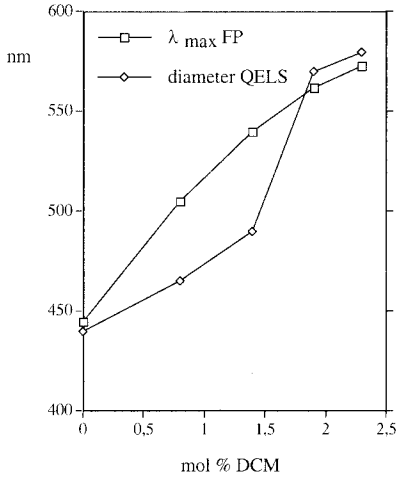

Figure 7.23. Solvent penetration and swelling of a 400 nm polystyrene latex by dichloromethane (DCM) as detected via the fluorescence shift of incorporated FP and by QELS.

Strong swelling sets in above 1.5 mol% DCM added to the aqueous dispersion medium. When the polymer particles are sparsely doped with FP they become brightly fluorescent and in the absence of DCM such a doped latex fluoresces at 445 nm, which is identical to the wavelength of FP in bulk polystyrene. This implies that the FP probes are embedded in the particles so as to be shielded from the aqueous medium. Upon addition of DCM the fluorescence shifts to the red as far as to 573 nm at 2.4 mol% signaling penetration of the solvent to the embedded FP molecules. Similar observations were made with other low molecular weight solvents. With DCM as well as with some other solvents the fluorescence of the embedded and non-extractable FP molecules is shifted to a position nearly identical to that for FP in the pure solvent.[51,62] This not only provides an optical probe for the solvent penetrability but, as can be seen from Figure 7.23, also allows detection of such solvent penetration at early stages where the size of the particles has not yet changed significantly. In later investigations these phenomena were e.g. exploited to study the crosslinking and drying of latex based coatings employing a crosslinker covalently tagged with MFP.[63] Also the kinetics of solvent penetration into latex particles was examined in more detail. While for the polystyrene latices used above penetration reaches a steady state within the mixing time, other latices show much slower solvent penetration especially when their T_g is high.[64]

When the FP labeled polystyrene latex used in Figure 7.23 is spread to a thin film and dried, a material is obtained of which the fluorescence is not only highly solvatochromic but also vapochromic. Thus contacting it with e.g. dichloromethane vapor rapidly and reversibly shifts its fluorescence from blue (445 nm) to orange green (573 nm) providing a nice class-room demonstration of a 'fluorescent nose'.[65]

7.3.5. Thin Film Electroluminescence, OLEDs and PLEDs

At present much interest is focussed on the development of light emitting diodes (LEDs) based on the electroluminescence of semiconducting thin organic films when sandwiched between a cathode consisting of a low work function metal (e.g. Al, Ca or Ba) and a transparent anode (mostly indium-tinoxide, ITO). Electroluminescence in such devices occurs if the energy, set free when holes and electrons injected at the anode and cathode respectively recombine, is sufficient to excite an embedded fluorophore or a fluorophoric polymer segment. We argued that the CT fluorescence of our FP and FT type probes in fact constitutes a hole-electron recombination, which is inherently radiative by it self. Therefore thin films of these probes in pure form or mixed with an appropriate semiconducting (but not necessarily electroluminescent) polymer might lead to small-molecule based LED's (OLEDs) or polymer based LEDs (PLEDs) respectively. The latter have the advantage that the thin film can be produced by spin coating, while for the former vapor phase deposition is required. Both types of devices have indeed been realised.[49,66,67] Vapor phase deposition of a homogeneous thin film, as required for the production of an OLED, turned out to be possible with FT as well as with its analogues **9** and **10** in which the cyanonaphthalene is substituted by the weaker acceptor pyrene.

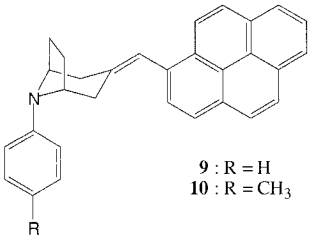

9 : R = H
10 : R = CH_3

PLEDs with polyvinylcarbazole (PVK) as the polymer matrix were produced from various CT probes including FT, **9** and **10** by spin coating solutions of PVK and a few weight % of the probe on an ITO anode and covering with a low work function metal anode.

The PLEDs as well as the OLEDs based on FT, **9**, and **10** show bright electroluminescence, as e.g. exemplified in Figure 7.6C, which is easily tuned in color by variation of the D and A moieties as well as of the embedding medium. Regrettably the operational lifetime of the LEDs reported until now is rather limited, which may be related to the chemical reactivity of the donor radical cation and acceptor radical anion species involved. Especially the successful construction of OLEDs based on pure thin layers of these D-σ-A probes, however, nicely supports the mode of operation proposed for creation of their CT excited state via an electrochemical pathway.

7.4. CONCLUDING REMARKS

The data discussed above constitute the main part of the results obtained until now with Fluoroprobe and Fluorotrope type D-σ-A probes since their discovery in 1984. These results demonstrated the extreme solvatochromism, thermochromism, and vapochromism of these probes and also their ability to detect subtle mobility changes in the surrounding matrix brought about by chemical, thermal or mechanical factors. It appears that these properties as well as their recently established electroluminescent properties have as yet not been exploited fully. The author hopes that this review will stimulate interest in further application and development of this type of probes.

7.5. ACKNOWLEDGEMENTS

The author thanks Dr. J.M. Warman and Dr. M.S. Frahn for making available the data plotted in Figure 7.22 and Dr. A.M. Brouwer for communicating unpublished results about the kinetics of solvent penetration in polymer latex particles.

7.6. REFERENCES

1. C. Reichardt, Solvatochromic Dyes as Solvent Polarity Indicators, *Chem. Rev.* **94**, 2319-2358 (1994).
2. C. Reichardt, *Solvents and Solvent Effects in Organic Chemistry*, chap. 6 (Wiley-VCH,Weinheim, 2003).
3. Z.R. Grabowski, K. Rotkiewicz, and W. Rettig, Structural Changes Accompanying Intramolecular Electron Transfer: Focus on Twisted Intramolecular Charge-Transfer States, *Chem. Rev.* **103**, 3899-4031 (2003).

4. P. Suppan, Solvatochromic Shifts: The Influence of the Medium on the Energy of Electronic States, *J. Photochem. Photobiol, A* **50**, 293-330 (1990).
5. H. Knibbe, *Charge-Transfer Complex Formation in the Excited State*, PhD dissertation (Free University, Amsterdam, 1969).
6. H. Oevering, J.W. Verhoeven, M.N. Paddon-Row, and J.M. Warman, Charge-transfer absorption and emission resulting from long-range through-bond interaction; Exploring the relation between electronic coupling and electron-transfer in bridged donor-acceptor systems, *Tetrahedron* **45**, 4751-4766 (1989).
7. J.W. Verhoeven, J. Kroon, M.N. Paddon-Row, and J.M. Warman, Kinetic and spectroscopic investigation of the influence of conformation and orbital-symmetry on long-range intramolecular donor-acceptor interaction, in: *Supramolecular Chemistry, NATO ASI Series Vol. 371*, edited by V. Balzani and L. De Cola, (Kluwer Academic Publishers, Dordrecht 1992) pp. 181-200.
8. G. Briegleb, *Elektronen-Donator-Acceptor-Komplexe* (Springer Verlag, Berlin, 1961).
9. A.W.J.D. Dekkers, J.W. Verhoeven, and W.N. Speckamp, On the nature of sigma-coupled transitions; through-bond interactions in 1-aza-adamantane derivatives, *Tetrahedron* **29**, 1691-1696 (1973).
10. P. Pasman, J.W. Verhoeven and Th.J. de Boer, Fluorescence of intramolecular electron donor-acceptor systems; the importance of through-bond interaction, *Chem. Phys. Lett.* **59**, 381-385 (1978).
11. P. Pasman, F. Rob and J.W. Verhoeven, Intramolecular charge-transfer absorption and emission resulting from through-bond interaction in bichromophoric molecules, *J. Am. Chem. Soc.* **104**, 5127-5133 (1982).
12. G.F. Mes, B. de Jong, H.J. van Ramesdonk, J.W. Verhoeven, J.M. Warman, M.P. de Haas, and L.E.W. Horsman- van de Dool, Excited-state dipole moment and solvatochromism of highly fluorescent rod-shaped bichromophoric molecules, *J. Am. Chem. Soc.* **106**, 6524-6528 (1984).
13. R.M. Hermant, N.A.C. Bakker, T. Scherer, B. Krijnen, and J.W. Verhoeven, Systematic Study of a Series of Highly Fluorescent Rod-Shaped Donor-Acceptor Systems, *J. Am. Chem. Soc.* **112**, 1214-1221 (1990).
14. T. Scherer, W. Hielkema, B. Krijnen, R.M. Hermant, C. Eijckelhoff, F. Kerkhof, A.K.F. Ng, R. Verleg, E.B. van der Tol, A.M. Brouwer and J.W. Verhoeven, Synthesis and exploratory photophysical investigation of donor-bridge-acceptor systems derived from N-substituted 4-piperidones, *Recl. Trav. Chim. Pays-Bas* **112**, 535-548 (1993).
15. S.V. Rodrigues, A.K. Maiti, H. Reis, and W. Baumann, Electro optical emission measurements on a non-conjugated bichromophoric donor-acceptor molecule, *Mol. Phys.* **75**, 953-960 (1992).
16. S. Depaemelaere, L. Viaene, M. van der Auweraer, F.C. De Schryver, R.M. Hermant, and J.W. Verhoeven, Non-radiative decay processes of the intramolecular charge transfer state in a rigid bichromophoric system, *Chem. Phys. Letters* **215**, 649-655 (1993).
17. R.J. Willemse, D. Theodori, J.W. Verhoeven, and A.M. Brouwer, Decay pathways of charge separated states in strongly fluoresecnt electron donor-acceptor compounds, *Photochem. Photobiol. Sci.* **2**, 1134-1139 (2003).
18. M. Bixon, J. Jortner, and J.W. Verhoeven, Lifetimes for radiative charge recombination in donor-acceptor molecules, *J. Am. Chem. Soc.* **116**, 7349-7355 (1994).
19. J.W. Verhoeven, T. Scherer, B. Wegewijs, R.M. Hermant, J. Jortner, M. Bixon, S. Depaemelaere, and F.C. De Schryver, Electronic coupling in inter- and intra-molecular donor acceptor systems as revealed by their solvent dependent charge-transfer fluorescence, *Recl. Trav. Chim. Pays-Bas* **114**, 443-448 (1995).
20. B. Wegewijs and J.W. Verhoeven, On long-range charge separation in solvent free donor-bridge-acceptor systems, in: *Advances in Chemical Physics, Vol. 106, Electron Transfer- From Isolated Molecules to Biomolecules, Part One*, Edited by J. Jortner and M. Bixon, (John Wiley & Sons, Inc., 1999), pp. 221-264.
21. R.M. Hermant, *Highly Fluorescent Donor-Acceptor Systems: Fundamentals and Applications*, PhD dissertation (University of Amsterdam, 1990).
22. B. Wegewijs, *Long-range charge separation in solvent-free Donor-bridge-Acceptor systems: Donor-bridge-Acceptor molecules in splendid isolation*, PhD dissertation (University of Amsterdam, 1994).
23. T. Scherer, *Conformational Dynamics of Fluorescent Exciplexes*, Phd dissertation (University of Amsterdam, 1994).
24. N.J. Turro, *Modern Molecular Photochemistry*, p. 90 (The Benjamin/Cummings Publ. Co., Menlo Park CA, 1978).
25. B. Wegewijs, T. Scherer, R.P.H. Rettschnick, and J.W. Verhoeven, Exciplex formation in jet-cooled donor-bridge-acceptor compounds incorporating bridges with three degrees of flexibility, *Chem. Phys.* **176**, 349-357 (1993).
26. W. Schuddeboom, T. Scherer, J.M. Warman, and J.W. Verhoeven, The formation of extended and folded charge separated states of donor-spacer-acceptor molecules with flexible and semi-rigid sigma-bond spacers, *J. Phys. Chem.* **97**, 13092-13098 (1993).

27. B. Wegewijs, A.K.F. Ng, and J.W. Verhoeven, Coulomb-induced intramolecular exciplex formation in semiflexible Donor-bridge-Acceptor co npounds in nonpolar solvents as a function of temperature, *Recl. Trav. Chim. Pays-Bas*, **114**, 6-12 (1995).
28. X.Y. Lauteslager, M.J. Bartels, J. J. Piet, J. M. Warman, J.W. Verhoeven, and A.M. Brouwer, Exploring the limits of the electrostatically induced conformational folding process in charge-separated excited states: retarding effect of long alkyl tails attached to the chromophores, *Eur. J. Org. Chem.*, 2467-2481 (1988).
29. X.Y. Lauteslager, I.H.M. van Stokkum, H.J. van Ramesdonk, A.M. Brouwer, and J.W. Verhoeven, Conformational dynamics of semiflexibly bridged D-A systems studied with a streak camera and spectrotemporal parametrization of fluorescence, *J. Phys. Chem. A*, **103**, 653-659 (1999).
30. G.F. Mes, *Photo-induced Electron-transport in Multichromophoric Systems*, PhD dissertation (University of Amsterdam, 1985).
31. R. Hoffmann, A. Imamura, and W.J. Hehre, Benzynes, dehydroconjugated molecules, and the interaction of orbitals separated by a number of intervening sigma-bonds, *J. Am. Chem. Soc.* **90**, 1499-1509 (1968).
32. J.W. Verhoeven, From close-contact to long-range intramolecular electron transfer, in: *Advances in Chemical Physics, Vol. 106, Electron Transfer- From Isolated Molecules to Biomolecules, Part One*, Edited by J. Jortner and M. Bixon (John Wiley & Sons, Inc., 1999), pp. 603-644.
33. A.M. Brouwer and R. Wilbrandt , Vibrational spectra of N,N-dimethylaniline and its radical cation. An interpretation based on quantum chemical calculations, *J. Phys. Chem.* **100**, 9678-9688 (1996).
34. A.M. Brouwer, Ab initio study of the structures and vibrational spectra of some diamine radical cations, *J. Phys. Chem. A* **101**, 3626-3633 (1997).
35. A.M. Brouwer, J.M Zwier, C. Svendsen, O.S. Mortensen, F.W. Langkilde, and R. Wilbrandt, The radical cation of N,N-dimethylpiperazine: dramatic structural effects of orbital interactions through bonds, *J. Am. Chem. Soc.* **120**, 3748-3757 (1998).
36. M. Goes, X.Y. Lauteslager, J.W. Verhoeven, and J.W. Hofstraat, A blue excitable Charge-Transfer fluorescent probe and its fluorogenic derivative, *Eur. J. Org. Chem.*, 2373-2377 (1998).
37. B. Krijnen, H.B. Beverloo, and J.W. Verhoeven , Conformational Effects of Through-Bond Interaction in N-Aryl-Piperidine Derivatives, *Recl. Trav. Chim. Pays-Bas* **106**, 135-136 (1987).
38. B. Krijnen, H.B. Beverloo, J.W. Verhoeven, C.A. Reiss, K.Goubitz, and D. Heijdenrijk, Effect of through-bond interaction on conformation and structure of some N-arylpiperidone and N-aryltropanone derivatives, *J. Am. Chem. Soc.* **111**, 4433-4440 (1989).
39. D.J.A. de Ridder, K. Goubitz, H. Schenk, B. Krijnen, and J.W. Verhoeven, Effect of Through-bond Interaction on Conformation and Structure in Rod-shaped Donor-Acceptor Systems; Part 2, Crystal Structures of Seven N-Aryltropan-3-one Derivatives, *Helv. Chim. Acta* **86**, 812-826 (2003).
40. R.P. Haugland, *Handbook of Fluorescent Probes and Research Chemicals, 5th edn.* (Molecular Probes Inc., Eugene OR, 1994), pp. 14-16, see also: http//www.probes.com/handbook.
41. H.J. Verhey, J.W. Hofstraat, C.H.W. Bekker, and J.W. Verhoeven, A fluorogenic charge-transfer polarity probe for the derivatisation of thiols and amines, *New J. Chem.* **20**, 809-814 (1996).
42. E.S. Gould, *Mechanism and Structure in Organic Chemistry* (Holt, Rinehart and Winston Inc., New York, 1959) p. 221.
43. M. Frahn, personal communication.
44. M.J. Bartels, M. Koeberg, and J.W. Verhoeven, Fluorescence Probing of Solvent Accessibility and Micropolartity on Silica and Alkylated Silica Surfaces, *Eur. J. Org. Chem.* 2391-2395 (1999).
45. E.R. Middelhoek, P. Vermeulen, J.W. Verhoeven, and M. Glasbeek, Picosecond time-dependent Stokes shift studies of fluoroprobe in liquid solution, *Chem. Phys.* **198**, 373-380 (1995).
46. E.R. Middelhoek, H. Zhang, J.W. Verhoeven, and M. Glasbeek, Subpicosecond studies of the solvation dynamics of Fluoroprobe in liquid solution, *Chem. Phys.* **211**, 489-497 (1996).
47. M. Goes, M. de Groot, M. Koeberg, J.W. Verhoeven, N.R. Lokan, M.J. Shephard, and M.N. Paddon-Row, Temperature dependence of charge-transfer fluorescence from extended and U-shaped donor-bridge-acceptor systems in glass-forming solvents, *J. Phys. Chem. A* **106**, 2129-2134 (2002).
48. E. Görlach, H. Gygax, P. Lubini, and U. Wild, Solvent relaxation of oxazine-4 in 2-methyltetrahydrofuran, *Chem. Phys.* **194**, 185-193 (1995).
49. M. Goes, *Photo- and Electroluminescence Generated by Intramolecular Charge Transfer*, PhD dissertation (University of Amsterdam, 2002).
50. L.W. Jenneskens, H.J. Verhey, H.J. van Ramesdonk, J.W. Verhoeven, K.F. van Malssen, and H. Schenk, Intramolecular Charge Transfer Fluorescence of 1-phenyl-4-(4-cyano-1-naphthyl methylene) piperidine as a sensor for phase transitions in the solid state, *Recl. Trav. Chim. Pays-Bas* **111**, 507-510 (1992).
51. H.J. Verheij, *Fluorescence Probing of Polymers*, PhD dissertation (University of Amsterdam, 1997).

52. L.W. Jenneskens, H.J. van Ramesdonk, H.J. Verhey, G.D.B. van Houwelingen, and J.W. Verhoeven, Discrimination between polarity and mobility effects on the charge-transfer fluorescence of Fluoroprobe in organic matrices, *Recl. Trav. Chim. Pays-Bas* **108**, 453-454 (1989).
53. L.W. Jenneskens, H.J. Verhey, H.J. van Ramesdonk, A.J. Witteveen, and J.W. Verhoeven, Intramolecular charge-transfer fluorescence of 1-phenyl-4-[(4-cyano-1-naphthyl)methylene]piperidine as a morphology probe in α,ω–diacetylpoly(ethylene glycol) matrices, *Macromolecules* **24**, 4038-4040 (1991).
54. L.W. Jenneskens, G.D.B. van Houwelingen, H.J. van Ramesdonk, H.J. Verhey, and J.W. Verhoeven, Intramolecular charge transfer fluorescence of 1-phenyl-4-(4-cyano-1-naphthylmethylene)piperidine as a mobility probe in α,ω-diacetyl poly(ethyleneglycols), in: *Integration of Fundamental Polymer Science and Technology-5*, edited by P.J. Lemstra and L.A. Kleintjes (Elsevier Applied Science, London and New-York, 1991), pp. 291-295.
55. L.W. Jenneskens, J.P.B. van Deursen, H.J. Verhey, H.J. van Ramesdonk, and J.W. Verhoeven, Molecular inhomogeneity of polymeric matrices, as detected by site directed fluorescent probes, *Appl. Fluor. Techn.* **3**, 11-15 (1991).
56. J.W. Hofstraat, J. Veurink, B. Gebben, H.J. Verheij, and J.W. Verhoeven, Charge-Transfer Fluorescent Probes Applied to the Characterization of Thermal and Mechanical Properties of Polymers, *J. Fluor.* **8**, 335-342 (1998).
57. H.J. van Ramesdonk, M. Vos, J.W. Verhoeven, G.R. Möhlman, N.A. Tissink, and A.W. Meesen, Intramolecular charge-transfer fluorescence as a mobility probe in (poly)methylmethacrylate, *Polymer* **28**, 951-956 (1987).
58. J.M. Warman, R.D. Abellon, H.J. Verhey, J.W. Verhoeven, and J.W. Hofstraat, Maleimido-fluoroprobe: A dual-purpose Fluorogenic Probe of Polymerization Dynamics, *J. Phys. Chem. B*, **25**, 4913-4916 (1997).
59. J.M. Warman, R.D. Abellon, L.H. Luthjens, J.S. Suykerbuyk, H.J. Verheij, and J.W. Verhoeven, In-situ monitoring of radiation-induced polymerisation of methylmethacrylate using fluorogenic molecular probes, *Nuclear Instruments and Methods in Physics Research B* **151**, 361-366 (1999).
60. M.S. Frahn, *Radiation-Induced Polymerization Monitored with Fluorogenic Molecular Probes*, PhD dissertation (Delft University of Technology, 2003).
61. C.P. Smyth in: *Physics and Chemistry of the Organic Solid State*, edited by D. Fox, M.M. Labes, and A. Weissberger (Interscience, New York, 1963), Vol. 1, p. 697.
62. H.J. Verhey, B. Gebben, J.W. Hofstraat, and J.W. Verhoeven, Detection of nanoscale events in dispersed polymer particles containing a charge-transfer fluorescence probe, *J. Polym. Sci.: Part A: Polym. Chem.* **33**, 399-405 (1995).
63. H.J. Verhey, L.G.J. van der Ven, C.H.W. Bekker, J.W. Hofstraat, and J.W. Verhoeven, Cross-linking and drying of a two-component waterborne coating monitored by a functionalized CT fluorescence probe, *Polymer* **38**, 4491-4497 (1997).
64. A.M. Brouwer, personal communication.
65. J.W. Verhoeven, unpublished results.
66. J. W. Verhoeven, M. Goes, J.W. Hofstraat, and K. Brunner, Electroluminescence of Charge-Transfer Fluorescent Donor-bridge-Acceptor Systems, *The Spectrum* **15-2**, 1-13 (2002).
67. M. Goes, J.W. Verhoeven, J.W. Hofstraat, and K. Brunner, OLED and PLED Devices Employing Electrogenerated, Intramolecular Charge-Transfer Fluorescence, *ChemPhysChem*. **4**, 349–358 (2003).